The Shelf Circulation of the Bellingshausen Sea
Third Revision

L. M. Schulze Chretien[1], A. F. Thompson[2], M. M. Flexas[2], K. Speer[3], N. Swaim[1], R. Oelerich[4], X. Ruan[5]. R. Schubert[3], C. LoBuglio[1]

[1]Marine Science Research Institute, Department of Biology and Marine Science, Jacksonville University, Jacksonville, Florida
[2]Environmental Science and Engineering, California Institute of Technology, Pasadena, California
[3]Geophysical Fluid Dynamics Institute, Department of Scientific Computing, Florida State University, Tallahassee, Florida
[5]Department of Earth, Atmospheric, and Planetary Sciences, Massachusetts Institute of Technology, Cambridge, Massachusetts
[4]Centre for Ocean and Atmospheric Sciences, School of Environmental Sciences, University of East Anglia, Norwich, United Kingdom.

Key Points:

- Warm Modified Circumpolar Deep Water flows towards the Bellingshausen Sea coast along the eastern edge of Belgica and Latady troughs.
- Waters with elevated meltwater concentrations flow away from the coast along the western sides of the two troughs.
- Estimates of heat and volume transports are comparable to other shelf seas in West Antarctica.

Corresponding author: Lena M. Schulze Chretien, `lschulz2@ju.edu`, `Marine Science Research Institute, Department of Biology and Marine Science, Jacksonville University`

Abstract

Over recent decades, the West Antarctic Ice Sheet has experienced rapid thinning of its floating ice shelves as well as grounding line retreat across its marine-terminating glaciers. The transport of warm Modified Circumpolar Deep Water (MCDW) onto the continental shelf, extensively documented along the West Antarctic Peninsula (WAP) and in the Amundsen Sea, has been identified as the key process for inducing these changes. The Bellingshausen Sea sits between the Amundsen Sea and the northern part of the WAP, but its oceanic properties remain remarkably under-studied compared to surrounding regions. Here, we present observations collected from a hydrographic survey of the Bellingshausen Sea continental shelf in austral summer 2019. Using a combination of ship-based and glider-based CTD and lowered ADCP observations, we show that submarine troughs provide topographically-steered pathways for MCDW from the shelf break towards deep embayments and ultimately under floating ice shelves. Warm MCDW enters the continental shelf at the deepest part of the Belgica Trough and flows onshore along the eastern side of the trough. Modification of these shoreward-flowing waters by glacial melt is estimated by calculating meltwater fractions using an optimal multiparameter analysis. Meltwater is found to be elevated at the western edge of both the Latady and Belgica troughs. Meltwater distributions, consistent with other diagnostics, suggest a recirculation in each trough with modified waters eventually flowing westward upon leaving the Belgica Trough. Our results show that the Bellingshausen Sea is a critical part of the larger West Antarctic circulation system, linking the WAP and the Amundsen Sea.

Plain Language Summary

Over the past decades large changes in the volume of the West Antarctic Ice Sheet have been observed. This has been attributed to a warm water mass, the Circumpolar Deep Water (CDW). This water has been observe along the West Antarctic Peninsula (WAP) and in the Amundsen Sea. The Bellingshausen Sea, located between the WAP and the Amundsen Sea, has exhibited similar rates of ice shelf thinning, yet remains remarkably under-studied compared to regions to the east and west. We present observations of the Bellingshausen Sea from early 2019. Using a combination temperature and velocity data are used to show that submarine troughs provide pathways for the warm water from offshore to reach the ice sheets. This takes place at the deepest part of the Belgica Trough and along the eastern side of the trough with a recirculation of this now slightly cooler water between the two troughs. The water originating from the ice sheets leaves the Bellingshausen Sea along the western side of the Belgica Trough before flowing west towards the Amundsen Sea. Our results show that this region is a critical part of the West Antarctic circulation system, linking the WAP and the Amundsen Sea.

1 Introduction

Oceanic processes in the Southern Ocean and along the Antarctic margins influence Earth's climate on a global scale. The upper Southern Ocean has persistently warmed over the last century (Gille, 2008), which has been accompanied by an increase in heat content of the West Antarctic continental shelf (Schmidtko et al., 2014) and by increased glacial melting (Pritchard et al., 2012; Cook et al., 2016). The thinning of floating ice shelves throughout West Antarctic coastal seas, which includes the Amundsen and Bellingshausen seas as well as the northern part of the West Antarctic Peninsula (WAP) (**Figure 1**), is one of the most dramatic signals of a changing climate (Cook & Vaughan, 2010; Adusumilli et al., 2020; Smith et al., 2020). Rapid loss of mass from the ice sheet, attributed to excess basal melt where warm ocean waters are delivered to the glaciers (Pritchard et al., 2012), is also associated with the retreat of grounding lines (Rignot et al., 2014) and the acceleration of ice sheet flow (Joughin et al., 2002). The rate of ice loss of the West Antarctic Ice Sheet (WAIS) is now estimated to be three times as large as it was in the 1990's

(IMBIE, 2018). A recent surface mass balance analysis found a more than ten-fold increase in mass loss from West Antarctica (from 12 $\pm$ 3 Gt/yr to 159 $\pm$ 8 Gt/yr) over the period 2009–2017, as compared to the period between 1979 – 1989. This increase is larger than the six-fold increase across all of Antarctica for these same time periods (Rignot et al., 2019). During the latest decade, ice mass loss was dominated by the Amundsen and Bellingshausen sectors, contributing more than 60% of the total mass loss around Antarctica (Rignot et al., 2019).

Accurate predictions for the future evolution of WAIS requires an understanding of controls on ocean heat content and circulation, properties that control ice-shelf basal melt rates. Yet, there remain many open questions about how the ocean circulation is likely to change due to the complexity of this region. First, the circulation of the Antarctic marginal seas depends on processes spanning a range of scales, including the large-scale flow of the Antarctic Circumpolar Current (ACC), the major subpolar gyres (Ross and Weddell Gyres), a rich boundary current system over the continental slope (Pea-Molino et al., 2016; Thompson et al., 2018), and intricate shelf circulations steered by complex bathymetry (*e.g.* Moffat et al. (2008); Brearley et al. (2019)). Furthermore, due to the lack of observations, it is difficult to ascertain changes from an uncertain baseline circulation strength and structure. The Bellingshausen Sea (BellS), the focus of this study, is at the confluence of a number of different circulation elements of varying scales and dynamics, but the region has remained nearly unobserved.

In the West Antarctic coastal seas, the penetration of warm Circumpolar Deep Water (CDW) on to the shelf is enhanced both by the proximity of the southern boundary of the ACC (Orsi et al., 1995) and a weak Antarctic Slope Front (ASF) on the upper continental slope (Jacobs, 1991; Whitworth III et al., 1998). In particular, along the western side of the Antarctic Peninsula, the southern boundary of the ACC, flowing to the northeast, extends up the continental slope and a westward-flowing Antarctic Slope Current (ASC) is absent (Moffat & Meredith, 2018). Once warm water accesses the shelf, it flows towards the coast, and, in the absence of major topographic barriers, delivers this heat to marine-terminating ice sheets, potentially contributing to basal melting. Along the WAP, CDW flows onto the shelf nearly unrestricted with exchange across the shelf break largely occurring at the Marguerite Trough and via coherent eddies (Moffat et al., 2009; Couto et al., 2017), although both the mean flow and eddies transport this water to the coast (Dinniman et al., 2011).

Farther to the west, in the Amundsen Sea, both observational (Walker et al., 2013) and numerical (Nakayama et al., 2013) evidence exists for a westward-flowing ASC near the shelf break. This change in the ASC between the WAP and Amundsen Sea suggests that a significant reorganization of the frontal structure over the continental slope occurs in the BellS sector (Thompson et al., 2020). The transport of heat on to the continental shelf in the Amundsen Sea, while still occurring primarily in glacially-carved troughs, differs from the WAP. The heat is supplied through an eastward-flowing undercurrent that sits over the continental slope and is largely controlled by the local wind stress (Walker et al., 2013; Dotto et al., 2019). It is unclear whether the WAP or Amundsen regime is more representative of heat transport on to the BellS shelf.

All ice sheets found along the coast of the BellS have experienced considerable volume loss (Paolo et al., 2015; Rignot et al., 2019; Adusumilli et al., 2020) and increased basal melt in the last decades (Rignot et al., 2013, 2019), with the possible exception of Abbot Ice Shelf. The ocean circulation close to the ice-shelf fronts in the eastern BellS, defined as the region that feeds the Wilkins, George VI, and Stange ice shelf cavities, has been studied previously (Jenkins & Jacobs, 2008; Padman et al., 2012), but the circulation and dynamics that influence the ice shelves in the western part of the BellS are not well known. For the purpose of this paper, we will refer to those ice shelves that are principally fed by the Marguerite and Latady troughs as the eastern BellS and those fed by the Belgica Trough as the western BellS (**Figure 1**). The Venable Ice Shelf, for example, is a smaller glacier by area, but has been estimated to have a rate of volume loss that is comparable to, or larger than, other ice shelves in the region (Rignot et al., 2013; Paolo et al., 2015).

The presence of warm CDW, referred to as Modified CDW (MCDW) due to mixing or modification processes occurring near the shelf break, over the BellS continental shelf was first identified by Talbot (1988). MCDW properties were found at the sea floor, which was explained by the absence of near-freezing, high-salinity water associated with the formation of deep water masses. The exchange of CDW across the shelf break is topographically-localized at glacially-carved troughs throughout West Antarctica (Dinniman & Klinck, 2004; Moffat et al., 2008; Savidge & Amft, 2009). The BellS has two major troughs, Belgica and Latady, shown in Figure 1. At the shelf break, the entrance to the Belgica Trough is located further to the west and closer to the Amundsen Sea and the Latady Trough is located closer to the WAP. Within Belgica Trough, a cyclonic circulation was inferred by Zhang et al. (2016), using data from instrumented seals and a Gade line analysis (Gade, 1979), with MCDW being carried onshore along the eastern side of the trough and meltwater carried offshore along the western side of the trough. These authors did not discuss the circulation in Latady Trough, and this region's contribution to heat transport towards the BellS ice shelves remains unconstrained. The generation of cyclonic circulations supported by glacially-carved troughs is a feature that is common throughout the WAP (Brearley et al., 2019; Savidge & Amft, 2009).

Coupled ice-ocean simulations carried out by Assmann et al. (2005) found the region to be dominated by a large-scale cyclonic circulation, although the model did not resolve circulation features in individual troughs. A strong coastal current formed the southern edge of this cyclonic circulation, extending from the BellS into the Amundsen Sea. The presence of a coastal current was also noted by Holland et al. (2010), originating along the WAP, flowing southward into the BellS. This coastal current has been reported to be a seasonal feature, disappearing in winter months (July – October) (Moffat et al., 2008). At the same time, sea ice conditions were suggested to be less variable in the BellS than in other regions, due to its location at the eastern edge of the Amundsen Sea low pressure system (Holland et al., 2010). Numerical models have further suggested an important role for the exchange of water properties and tracers between the various seas of West Antarctica. In particular, Nakayama et al. (2014) found that basal melting in the BellS can be a driving force in the freshening of the Ross Sea, a source region of deep water formation.

The transport pathways and fate of glacial meltwater that enters the ocean from basal melting of ice shelves remains a compelling and open topic. A broad freshening of the polar seas around Antarctica has been found in models as well as observations and coincides with the increased ice shelf mass loss (Schmidtko et al., 2014; Rye et al., 2014; Richardson et al., 2005; Swart & Fyfe, 2013). The vertical distribution of this meltwater in the water column and its impact on shelf and larger-scale circulation remains uncertain. Most observations suggest that the freshening has a subsurface signature, often up to several hundred meters deep, consistent with the outflow from the base of the ice shelves (Jenkins & Jacobs, 2008; Biddle et al., 2017; Loose et al., 2009; Kim, 2016; Adusumilli et al., 2020). However, glacial melt can also be redistributed within the water column by mixing processes, including those related to strong hydrographic fronts that develop at the ice shelf face (Naveira-Garabato et al., 2017). The depth and density classes over which glacial melt is found in the BellS suggest an important role for meltwater in modifying buoyancy and supporting an overturning circulation (Savidge & Amft, 2009; Moffat et al., 2008).

Recently acquired data from the BellS provide new insights into the circulation structure from the shelf break to the coast. In this manuscript we introduce our data and methods in Section 2; water mass properties, velocities, meltwater fractions and heat transports on the shelf are analyzed in Section 3. Section 4 assesses similarities and differences between the BellS circulation and observations and simulations of neighboring regions in West Antarctica. A summary is presented in Section 5.

2 Data and Methods

2.1 NBP19-01 Cruise data

The observations used in this study were collected aboard the R/V Nathaniel B. Palmer as part of the TABASCO (NBP19-01, Transport of the Antarctic Peninsula and Belingshausen Sea: Antarctic Slope Current Origins) research cruise. During the cruise, 56 temperature and salinity (CTD) profiles were collected in the BellS between 27 December, 2018 and 8 January, 2019. Stations 3 – 56 were organized into a series of transects. Two transects spanned the continental slope and shelf break: stations 3 – 10 located to the west of Belgica Trough and stations 51 – 56 starting from the eastern edge of the Latady Trough. The remaining stations (St 11 – 50) were located over the continental shelf (**Figure 1**). CTD data were acquired using a SBE-11+ (V2) deck unit and two SBE3plus temperature sensors. Velocity measurements were collected at each station using a RDI Workhorse Sentinel downward-looking Lowered Acoustic Doppler Current profiler (LADCP). The LADCP was configured to record velocity in 8 m bins and processing involved the use of both the hydrographic data and shipboard ADCP data, following Thurnherr et al. (2010).

Water samples were collected at each station, and the salinity was calibrated using a Guildline PortaSal 8410A. Winkler analysis was not performed during the cruise. No drift was observed between the two oxygen sensors on the CTD over the duration of the data collection in the BellS, but there was an offset of 12.05 μmol kg^{-1} between the two sensors. In the absence of direct calibration, we relied on comparisons between an offshore CTD profile and a nearly contemporaneous CTD profile obtained during the 2019 LTER survey (within 14 km and two weeks). Below 1500 m, the offset was roughly 12.8 μmol kg^{-1} for the first sensor, and 3.7 μmol kg^{-1} for the second sensor. After calibration and correction for offsets, the temperature, conductivity and oxygen sensors are expected to have an accuracy of 0.001°C, 0.0003 S m^{-1}, and 2% of saturation, respectively. More details can be found in the cruise documentation (`http://web.gps.caltech.edu/~andrewt/publications/TABASCO.pdf`).

All CTD data were processed following the guidelines in McTaggart et al. (2010). The hydrographic data were used to analyze temperature, salinity and density distributions, as well as to calculate meltwater fractions contained in the water column. We calculated geostrophic velocities, which were referenced to the de-tided LADCP data. Details of data processing are provided in the TABASCO project cruise report. Data from NBP1901 are archived at the National Center for Environmental Information and have the NCEI Accession Number 0210639.

In addition to the ship-based measurements, two ocean gliders, Seagliders, were deployed during the cruise. The first glider (SG621) was deployed on 27 December, 2018, offshore of the shelf break near Peter I Island (67.95°S, 87.88°W). We attempted to sample the continental slope and shelf break to the west of Belgica Trough with this glider, but had limited success due to sea ice extent; we do not discuss data from this glider further. The second glider (SG539) was deployed just offshore of the shelf break near Marguerite Trough on 19 January, 2019 (66.67°S, 72.50°W); a 2000 m CTD cast was completed immediately after deployment that was used for calibration purposes. After sampling the mouth of the Marguerite Trough, this glider moved south and sampled across the mouth of the Latady Trough. In this study, we made use of the last 106 dives collected by SG539 (**Figure 1**). The glider completed V-shaped dives to a depth of 1000 m or to within 15 m of the seafloor, if shallower than 1000 m. Surfacing locations were separated by roughly 4 km, and as little as 1 km when the glider was over the continental shelf. While diving, the glider collected measurements of temperature and salinity with a Seabird CTSail every

5 seconds, or roughly every 1 m vertically. The data were later processed using the UEA Seaglider Matlab Toolbox (www.byqueste.com/toolbox.html) that also includes a thermal lag correction following Garau et al. (2011). For this study we focused on temperature and salinity data from the glider; following calibration, temperature and salinity are accurate to 0.01°C and 0.01 g kg^{-1}, respectively. Measurements were then averaged in 10 m depth bins and interpolated onto a 10 km horizontal grid. Due to problems with the compass, no depth-averaged velocities were obtained. The barotropic nature of the currents in this region (shown below) means that non-referenced geostrophic velocities are of limited use in calculating fluxes across the glider section.

2.2 Velocity corrections and transports

The LADCP velocity data were de-tided using tidal velocity output from the Circum-Antarctic Tidal Simulation (CATS2008, Howard et al. (2019)). This is a high-resolution inverse model based on a uniform grid size of 4 km. It includes cavities under the floating ice shelves (Padman et al., 2002) and predicts tidal effects including surface heights, tidal current velocities and transports. We subtracted the predicted CATS2008 tidal velocities from the LADCP data. The tidal velocities in the BellS were relatively small (less than 5 cm s^{-1}) compared to the LADCP velocities; removal of tidal contributions did not significantly impact the results presented here (see **Figure S1**).

The combined use of the CTD and LADCP data allowed for the calculation of absolute geostrophic velocities. We first used the hydrographic data for each station pair to estimate geostrophic shear. The LADCP data were rotated to be along/across each station pair. The reference velocity was then calculated by minimizing the root mean square difference between the referenced geostrophic flow and the mean of the two rotated LADCP profiles for each station pair. Due to the barotropic nature of the flow, we calculated the reference velocity using the full water column depth. The resulting referenced geostrophic velocities were used to calculate volume and heat transports across the sections **Figure S2**. Transport contributions from bottom triangles, while generally small over the shelf due to the relatively flat topography (compared to the slope sections), were included using two methods: (1) a linear interpolation to the bottom of the velocity in the last common bin between each station pair, (2) a linear interpolation to zero at the bottom from the last common bin between each station pair. Here, we used method (1), which modified the volume transport by less than 5% as compared to not including bottom triangles, in the transport estimates discussed in section 3.4. Volume transports calculated using absolute geostrophic velocities, as opposed to the LADCP velocities alone, provide a more synoptic representation of the circulation since the LADCP captures ageostrophic components, e.g. tides and inertial oscillations, that typically exhibit higher frequency variability.

The heat flux F_h is defined as:

$$F_h = \rho C_p v \left(\theta - \theta_f\right), \tag{1}$$

and the heat transport Q_h across a hydrographic section is calculated as:

$$Q_h = \int_{x_w}^{x_e} \int_{-H}^{0} \rho C_p v \left(\theta - \theta_f\right) \, \mathrm{d}z \, \mathrm{d}x. \tag{2}$$

Here C_p is the specific heat capacity of sea water, calculated for each profile (J kg^{-1} K^{-1}), ρ is the average density of the station pair, θ is potential temperature referenced to the surface, θ_f is the freezing point potential temperature (a function of both salinity and pressure), and v is the referenced geostrophic velocity perpendicular to the station pair. The integrals in the heat transport calculation were taken in the vertical from the seafloor ($z = -H$) to the surface ($z = 0$) and in the horizontal from the western edge to the eastern edge of the two trough sections, x_w and x_e, respectively. Stations 11 – 22 correspond to the transect that spans the Belgica Trough near the shelf break, and stations 27 – 33 and 42 – 45 together cross both the Belgica and Latady troughs further to the south. We refer to the latter as the mid-shelf section below.

While multiple factors could contribute to error in our volume and heat transport estimates, we will assume that the dominant contribution comes from the LADCP velocity profiles, due to the strong barotropic nature of the flow. Following (Thurnherr et al., 2014), we assume the LADCP velocity error is no more than 3 cm s^{-1}. An upper bound on the error estimate for the volume flux would then simply use a 3 cm s^{-1} velocity, multiplied by the area of each station pair to calculate cumulative transports across the sections. The error associated with approach is typically $O(0.1)$ Sv for each station pair, dependent on the depth and width of the station pair. However, across each of the cross-trough sections there is both inflow and outflow, such that the cumulative transport has a large cancellation between positive and negative transports, and the error is large compared to the cumulative transport. For the Belgica Trough section, the total volume transport is 0.46 Sv ± 3.5 Sv, and for the mid-shelf section, the total volume transport is -0.66 Sv ± 4.9 Sv. To arrive at a more realistic error estimate, we chose to randomly sample an error reference velocity for each station pair from a Gaussian distribution with a standard deviation of 3 cm s^{-1}. The cumulative transports across each section were then calculated 10,000 times and the transport error was determined as the root mean square of these values. With this approach, we obtained cumulative volume transports across the Belgica Trough section (St 11 – 22) of 0.46 Sv ± 0.36 Sv and across the mid-shelf section (St 27 – 33 and 42 – 45) of -0.66 Sv ± 0.51 Sv. The same approach was used to calculate errors in the heat flux calculations. Using a constant error of 3 cm s^{-1}, the Belgica Trough and mid-shelf sections have heat transports of 43.2 GW ± 792 GW and -169 GW ± 1100 GW, respectively. Using the "error sampling" approach described above, this becomes 43.2 GW ± 82.5 GW (Belgica Trough) and -169 GW ± 118 GW (mid-shelf).

Below, we discuss the heat content of the MCDW layer at individual stations, which is calculated as:

$$\mathcal{H}_{MCDW} = \rho C_p \int_{z_{d|\theta=1.1^\circ\mathrm{C}}}^{z_{|\theta=1.1^\circ\mathrm{C}}} \theta \, \mathrm{d}z, \tag{3}$$

where C_p and ρ are the specific heat capacity of sea water and density calculated for the MCDW layer. The MCDW layer is defined as water with θ >1.1°C. Each profile was integrated vertically from the deepest 1.1°C isotherm, or the seafloor if a deep 1.1°C isotherm is not present (e.g. at St 21 or 27), to the depth of the shallowest 1.1°C isotherm.

2.3 Meltwater calculations

For this study, meltwater fractions were calculated using an optimum multiparameter analysis (OMP) (Tomczak, 1981; Loose & Jenkins, 2014; Biddle et al., 2017; Beaird et al., 2015; Loose & Jenkins, 2014). The method relies on a set of overdetermined equations that calculates the relative partitioning of observed water mass properties into a given number of end-member water masses with fixed hydrographic properties. An advantage of the OMP analysis, compared to a traditional mixing-line approach, is that it accounts for variations in the end-member properties arising from both instrument errors and environmental conditions. This variability is encapsulated in weighting factors.

The OMP method in this study was applied to three available observed tracers: temperature, salinity, and dissolved oxygen. Because surface waters (Antarctic Surface Water in this region) cover a wide range of possible end-member values due to direct surface forcing, the upper 150 m are excluded from the OMP analysis. This exclusion of surface data is common around the Antarctic margins (Biddle et al., 2017, 2019). We identified three end members: Winter Water (WW), Modified Circumpolar Deep Water (MCDW) and Glacial Melt Water (MW). The water mass distribution over the continental shelf is described in detail in section 3.1.

Mathematically, the OMP analysis involves a system of linear equations relating the end member properties to each observed tracer value by estimating the relative contribution from each water mass. A final equation arises from the constraint that the sum of the water mass fractions must equal one. The full system of linear equations can be written as:

$$\mathbf{Ax} - \mathbf{d} = \mathbf{r}. \tag{4}$$

Here, $\mathbf{A}$ is the matrix of the end-member tracer values as well as the mass conservation equation, $\mathbf{x}$ is the vector of water mass fractions (the values to be calculated), $\mathbf{d}$ is the vector of observed tracer values, and $\mathbf{r}$ is the vector of residuals between the observed tracer values and the linear solution. To solve equation (4) for $\mathbf{x}$, we followed Tomczak (1981) and inverted the over-determined system to minimize $||\mathbf{r}^2|| = \mathbf{r}^T\mathbf{r}$ with a non-negativity constraint on $\mathbf{x}$:

$$\mathbf{r}^T\mathbf{r} = (\mathbf{Ax} - \mathbf{d})^T \, \mathbf{W}^T\mathbf{W} \, (\mathbf{Ax} - \mathbf{d}) \, . \tag{5}$$

In equation (5), both $\mathbf{A}$ and $\mathbf{d}$ are normalized and weightings W_j are introduced, as described by Tomczak (1981). In this study, $j = [1, 2, 3]$ represents each tracer; there is a fourth parameter, W_4 that provides the weighting for the mass conservation constraint. The first three weightings were determined by calculating the variance of the end-member tracer values (σ_j) and dividing by the square of the uncertainty of that tracer across all end-members (ϵ_j),

$$W_j = \frac{\sigma_j^2}{\epsilon_j^2}. \tag{6}$$

End-members used in this calculation (MCDW, WW, and MW) are listed in **Table 1**, together with their tracer properties and uncertainties that were used to weight each tracer. The meltwater endpoints used in this study are theoretical values also used in Biddle et al. (2017) and Nakayama et al. (2013), where the θ is a theoretical value that accounts for the freezing enthalpy. For dissolved oxygen we used end members and data consistent with the second sensor (see Section 2.1). Note that in many previous studies the weighting value for the mass conservation constraint, W_4, was not reported. We found a strong sensitivity to this choice, which was not constrained by equation (6). We chose a value for W_4 (Table 1) that ensured that any deviation in the sum of the water mass fractions away from 1 was at least an order of magnitude smaller than the meltwater fraction itself. The values in $\mathbf{W}$ for $j = [1, 2, 3]$ were similar to Biddle et al. (2017), although we used a larger value of W_4 (Biddle, personal communication).

Uncertainties in the meltwater fractions ($\mathbf{x}$) calculated from equation (5) were assessed using a Monte Carlo simulation. For this, equation (5) was solved 10,000 times with each end-member property in $\mathbf{A}$ replaced by a perturbed value selected from a normal distribution of the mean values A_{ij} modified by the largest uncertainty associated with each tracer, represented by ϵ_j. This resulted in 90,000 perturbed realizations of end-member properties. MW fraction concentrations were reliable to $\pm$ 1.1 g kg^{-1}. This error is comparable to the $\pm$ 1 g kg^{-1} value reported by Biddle et al. (2017), but larger than the 0.5 g kg^{-1} error values that are typical of studies that include constraints from noble gases (Biddle et al., 2019; Beaird et al., 2015).

Finally, due to the lack of calibration in the dissolved oxygen measurements, we performed additional sensitivity tests for the OMP analysis. First, we tested the impact of the offset between sensors 1 and 2, by carrying out the OMP analysis with both oxygen sensors with suitably modified end members to account for the sensor offset. In this case, while the magnitude of the meltwater fraction did change, particularly in the easternmost stations (44 – 46), the large-scale distribution and the peak magnitudes were similar (**Figure S3 a,b**). Next, we re-calculated the meltwater distribution using the OMP analysis where the weight associated with the dissolved oxygen tracer was reduced by a half (**Figure S3c**) and to zero (**Figure S3d**). Again, the spatial distribution in meltwater fraction remained similar although the magnitude decreased as the influence of oxygen on the OMP analysis was reduced.

These sensitivity tests were carried out due to our limited ability to directly calibrate the oxygen sensors. In summary, we find that the vertical structure of meltwater distribution (described in section 3.3) shows some sensitivity to the weighting of the oxygen data, but the horizontal distribution of the meltwater fractions over the continental shelf are relatively insensitive to these changes. Accordingly, due to the uncertainty in the dissolved oxygen measurements, we put emphasis on the spatial distribution of the meltwater fractions, as opposed to their absolute magnitude.

3 Results

3.1 Water mass distribution

Water masses over the BellS continental shelf are organized in a two-layer configuration (**Figure 2a** and **Figure 3**). The upper layer consists of Antarctic Surface Water (AASW, $\gamma^n < 28.00$) and Winter Water (WW, $\gamma^n < 28.00$, $\theta = \theta_{min}$; Table 1), the sub-surface remnant of cold, winter AASW after summer warming caps the ocean surface (Mosby, 1934). The lower layer consists of Modified Circumpolar Deep Water (MCDW, $28.00 < \gamma^n < 28.27$, $\theta > 1.1$°C) (Whitworth III et al., 1998). The origin of MCDW is Circumpolar Deep Water (CDW, $28.00 < \gamma^n < 28.27$, $\theta = 1.85$°C) offshore from the slope. This modification involves both mixing processes that are localized to the upper continental slope and water mass transformation processes that occur through interaction with ice shelves and, potentially, sea ice formation if convection due to brine rejection penetrates deep enough in the water column. The permanent pycnocline separates AASW/WW from MCDW.

The warmest (least modified) MCDW ($\theta > 1.4$°C) is found at the shelf break, at the eastern side of Latady Trough (300 m – 400 m deep) (**Figure 3a**). MCDW of $\theta > 1.2$°C is found over the entire Latady Trough, and over the eastern side of Belgica Trough. The temperature maximum in the MCDW layer is generally found ∼200 m above the bottom (trough depth 650 m). Since the offshore CDW temperature maximum is found at roughly 400 m (Thompson et al., 2020), this indicates that CDW flows topographically unconstrained on to the shelf.

Above MCDW, AASW and WW occupy the upper 200 m in Belgica and Latady troughs. While WW on the eastern side of Latady Trough is capped by relatively warm AASW (∼ -0.4°C), surface waters over the rest of the continental shelf were relatively cold (< -1.4°C) during the TABASCO survey. The temperature minimum of the WW lies between 50 m and 100 m. The permanent pycnocline, associated with the 27.8 kg m^{-3} isopycnal, tilts across Belgica Trough at the shelf break (about 300 m deep at the western side of the trough as compared to 100 m deep at the eastern side), which is consistent with a cyclonic, baroclinic circulation inside Belgica Trough. The permanent pycnocline shows a doming structure in Belgica and Latady troughs in the mid-shelf transect (**Figure 3b**), indicating a general cyclonic circulation inside these troughs.

Analysis of temperature and salinity properties of MCDW (**Figure 4)** provides insight into the circulation of Belgica and Latady troughs. Less-modified MCDW properties are observed over the eastern side of Latady Trough (**Figure 4d**), extending southwards along ∼ 80°W (**Figure 4c,d**). The relatively colder MCDW over the mid-shelf Latady Trough (**Figure 4c**) suggests modification takes place near the coast before this water is directed back offshore along Latady and Belgica troughs. The coldest MCDW (1.25°C, **Figure 4d**) is found at the shelf break, at the westernmost edge of Latady Trough, completing the clockwise circulation inside Latady Trough.

In Belgica Trough, MCDW with elevated θ and S values (1.4°C, **Figure 4b**), corresponding to direct offshore CDW intrusions, are found over the eastern side of the trough (**Figure 4b**). These intrusions feed the center of the trough with warm MCDW (1.35°C, **Figure 4a**). Moving south, at the mid-shelf section, MCDW with colder temperatures than those observed at the shelf break (1.25°C, **Figure 4a,b**) is found along the eastern side of Belgica Trough. This water shares the same θ-S properties as MCDW along the western edge of Latady Trough (**Figure 4c**), which suggests that there is exchange between the two troughs and a modification of properties between the shelf break and the coast in Belgica Trough. Closer to the coast, strong modification occurs near Venable Ice Shelf (**Figure 4a**), giving rise to a colder and fresher version of MCDW (S=34.7, $\theta \sim 1.1$°C) that preserves these characteristics as it flows away from the ice shelf and back towards the shelf break along the western side of Belgica Trough (**Figure 4a**). This completes a clockwise circulation of MCDW inside Belgica Trough.

Winter Water properties also show interesting modifications (**Figure 5**). In Latady Trough, the WW θ_{min} is warmer at the shelf break (-1.55°C, **Figure 5d**). Colder WW (-1.8°C) is found inside Latady Trough, and over the western side of Belgica Trough (**Figure 5b,c**). The coldest and saltiest WW is found at the western side of Belgica Trough (**Figure 5a**). The high salinity of these waters, with respect to WW measured upstream close to Venable Ice Shelf, suggests the influence of local sea ice formation.

3.2 Velocities

Inferences about the circulation structure gained from the temperature and salinity distributions presented in section 3.1 are complemented by velocity observations from both direct LADCP measurements and referenced geostrophic velocities. Together, these show a consistent picture of MCDW flowing on to the continental shelf and towards the BellS ice shelves with both Belgica and Latady troughs, predominantly along the western side, with an offshore flow of colder, modified waters on the western side of these troughs (**Figure 4 and Figure 6**).

A dominant feature of the circulation is its strong barotropic character, especially near the continental shelf break. At the shelf-break section across Belgica Trough (**Figure 6a**), the core of warmest water flows onshore at the deepest part of the trough, located roughly at the trough's center, and is associated with velocity peaking at nearly 15 cm s^{-1} (stations 17 – 20). Note that acquisition of this section, as well as the other cross-trough sections, took roughly one full day to complete. The onshore flow is sandwiched between two strong regions of offshore flow. To the east, there is a strong ($>$ 15 cm s^{-1}) offshore flow found over the eastern slope of Belgica Trough (stations 20 – 22). This outflow is associated with a strong lateral gradient in temperature at roughly 400 m depth, suggesting that the outflow is not part of a recirculation or eddy localized to the shelf break. Instead, this difference in temperature likely arises due to the outflow of more modified MCDW from the offshore limb of the cyclonic circulation in the Latady Trough (section 3.1). The shallow bathymetry that separates the mouths of Belgica and Latady troughs may help focus and strengthen the outflow here. On the western side of Belgica Trough (stations 11 – 17), there is a net outflow that is weaker than the outflow on the eastern side, but is also confined to narrow boundary currents.

Due to a compass error, the glider did not produce accurate depth-averaged currents at the mouth of Latady Trough and it is difficult to infer circulation here without knowing the barotropic component of the flow. Nevertheless, from the glider hydrographic data, there is an indication of onshore flow at the eastern edge of Latady Trough, which could be caused by flow across the shelf break that feeds the cyclonic circulation of the trough or by a southern extension of the ACC across the shelf break.

The mid-shelf section that spans Belgica and Latady troughs (**Figure 6b**), is characterized by velocities with smaller magnitudes as compared to the shelf break section, with all observed LADCP velocities less than 10 cm s^{-1}. Across this mid-shelf section, the flow is organized into single regions of inflow and outflow in each trough. In both troughs, the inflow is confined to the eastern side and the outflow is located on the western side, consistent with the cyclonic circulation inferred by Zhang et al. (2016). The velocity structure in Latady Trough has a more baroclinic structure than in Belgica Trough, with stronger flows occurring below $\sim$ 300 m depth.

A near-shore hydrographic section was collected at the face of Venable Ice Shelf, consisting of four stations. The depth-averaged flow from these stations shows a strong offshore velocity moving away from the ice shelf along the topographic saddle separating Eltanin Basin to the east and another deep basin to the west in front of Venable Ice Shelf (**Figure 6c**).

Due to the barotropic nature of the flow in the troughs, referencing geostrophic velocities to either the Shipboard ADCP or Lowered ADCP data is essential for estimating the magnitude of the absolute geostrophic transport. One difference between the geostrophic velocities and the velocities derived from the LADCP is that the onshore flow is bottom-intensified in the former (**Figure S2 b,c**). The referenced geostrophic velocities also show less structure on the western side of Belgica Trough shelf-break section, such that all of the flow is offshore to the west of the maximum trough depth. The regions of narrow onshore and offshore flow in the LADCP data may indicate a coherent eddy or may be related to temporal variability that has a stronger signature in the barotropic component of the flow.

3.3 Meltwater Distributions

Hydrographic and velocity observations support the picture of coherent cyclonic circulations that are steered by and confined within the two major troughs in the BellS. The estimates of meltwater (MW) fractions presented in this section further support these features. Based on the OMP analysis (**Section 2.3**), the distribution of MW fraction is presented for the mid-shelf section that spans the Belgica and Latady troughs and for the short section that extends away from Venable Ice Shelf (**Figure 7**). To emphasize spatial differences across the Bells, the distribution of MW fraction is also shown for the two cross-slope sections on the eastern and western sides of the BellS (**Figure 8**). In these figures, MW fractions are presented both as a function of depth and as a function of neutral density γ^n.

For all CTD stations over the continental shelf, the $\gamma^n = 28.0$ kg m^{-3} neutral density surface, roughly located at 400 m depth and associated with the upper boundary of MCDW, marks a transition in MW fraction, with MW found almost exclusively above this level. The largest MW fraction values are found in front of the Venable Ice Shelf, with the largest magnitude at station 39, immediately in front of the ice shelf face (**Figure 7c**). The peak in MW concentration at this station is aligned with the 0°C isotherm, which corresponds to the 27.86 kg m^{-3} isopycnal and a depth of 350 m. This isotherm/isopycnal shoals moving away from the ice shelf and the peak MW fraction tracks this change; the peak MW value is found at 200 m at station 34, 75 km away from the ice-shelf face. The offshore transport of this MW anomaly is largely adiabatic as shown by mapping MW to density coordinates (**Figure 7d**). This subsurface peak in MW is consistent with an outflow from Venable Ice Shelf cavity, where the draft of the ice shelf is estimated to be 280 m on average (Morlighem et al., 2019), although there are large MW fraction values at shallower depths that may arise from vertical mixing. At station 39 (and further offshore), the change in MW fraction with depth above the 0° isotherm is non-monotonic, which may be a signature of lateral stirring carrying water both towards and away the ice-shelf face. Finally, an additional, shallower MW fraction maximum is found at stations 34 and 35 at a depth of ~150 m, corresponds to a density of $\gamma^n = 27.75$ kg m^{-3}.

At the mid-shelf section, the maximum MW fractions are located in two separate cores along the western side of Belgica Trough, peaking at 7 g kg^{-1} at stations 29 – 33 (**Figure 7a,b**). One core is located at the western edge of the trough (station 33) and at a neutral density of $\gamma^n = 27.88$ kg m^{-3} (280 m); this density surface is consistent with the outflow from the Venable Ice Shelf. A second, shallower core at $\gamma^n = 27.80$ kg m^{-3} (150 m), is found further east at stations 30 – 32. The former is largely consistent with the properties of the MW core in front of the Venable Ice Shelf, whereas the shallower core is found at similar depths and density surfaces as MW at stations 34 and 35. MW fractions are also elevated in the upper water column (~150 m and above $\gamma^n = 27.9$ kg m^{-3}) on the western side of Latady Trough (St 42 – 43). Independent of the vertical structure, in both troughs the locations of elevated MW fractions are found on the western side of the trough and are collocated with regions of offshore flow (**Figure 6**), suggesting an export of MCDW that has been glacially-modified.

Variations in the meltwater distribution extend all the way to the shelf break as indicated by cross-slope sections at the western and eastern extent of the BellS (**Figure 8**). Meltwater fractions are highest at the western edge of Belgica Trough (**Figure 8a,b**), with fractions of 9 g kg^{-1} — nearly twice the values found on the eastern side of the BellS (**Figure 8c,d**). On the eastern side, the MW maximum is located at offshore stations (St 54 – 56), over the continental slope, while the MW maximum at the western section is adjacent to the continental shelf (St 7 – 11), extending offshore above the 0°C isotherm. For both sections, the core of MW is located close to 150 m, and within density classes lighter than $\gamma^n = 27.85$ kg m^{-3}. In the western cross-slope section (**Figure 8a,b**), a sharp meltwater front is established, bounded by the southern boundary of the ACC. Elevated MW fractions at the western side of Belgica Trough are consistent with inferred MW distributions based on coarser hydrographic profiles obtained from instrumented seals by Zhang et al. (2016).

The layer in which MW fractions are found accounts for ~400 m of the water column in the western Belgica Trough as compared to only ~100-175 m in the eastern Belgica Trough and in Latady Trough (**Figure 9**). The MW content is largest in front of Venable Ice Shelf, as also seen in the hydrographic sections above. Integrating the MW content vertically in the water column results in peak values near the coast of 3.5 m. MW content across the shelf-break and mid-shelf sections in both troughs is lower, around 0.9 – 1.3 m, but with elevated values in the western Belgica Trough, ~2.25 m. MW content is also elevated west of Belgica Trough, over the continental shelf break. Here, positive MW anomalies are found in a narrow band between the 1000 – 2000 m isobath. This further supports the idea that this region is the primary export site of modified waters from the BellS (Thompson et al., 2020). Within Latady Trough, MW is higher along the eastern side of the trough despite the cyclonic flow structure discussed above. One possible explanation for this elevated MW could be a southward extension of the Antarctic Peninsula Coastal Current. This coastal current is known to transport glacial runoff along the WAP, and hence could contribute to the relatively large NW content found in the eastern Latady Trough (Moffat & Meredith, 2018). The lower value of MW on the western side of Latady Trough, on the other hand, may indicate that only a small amount of MW is transported towards the shelf break via Latady Trough. Some of this MW might be diverted toward Eltanin Basin and Belgica Trough, and may further explain the elevated MW signal in the western Belgica Trough and over the western BellS shelf.

3.4 Volume and heat transports

Volume and heat transports were calculated at the mouth of Belgica Trough and at the mid-shelf section spanning Belgica and Latady troughs (**Figure 10**). The largest offshore transports are found at the western side of the Belgica trough (1.1 Sv ± 0.3 Sv between stations 11 – 13) and close to the gap connecting Belgica to Latady Trough (0.65 Sv ± 0.16 Sv between stations 20 – 22). The net transport across the mouth of Belgica Trough is nearly closed (0.46 Sv ± 0.36 Sv net offshore transport).

Transports across the mid-shelf section are generally weaker than those across the shelf break section. A weak onshore transport of 0.2 Sv ± 0.3 Sv was measured at the deep, eastern-most station-pairs of Latady Trough (**Figure 10b**, middle panel, stations 44 – 46). This suggests that we may be missing a potentially narrow onshore current on the eastern side of the trough. As can be seen in the bathymetric profile (**Figure 10b**, top panel), the mid-shelf section was not properly closed; thick sea ice prevented the ship from closing the section across Latady Trough. The offshore flow on the western side of Latady trough was 0.41 Sv ± 0.36 Sv (**Figure 10b**, middle panel). The volume transport towards the coast on the eastern side of the Belgica Trough is 1.2 Sv ± 0.6 Sv. On the western side of Belgica Trough, the volume transport away from the coast is 0.6 Sv ± 0.16 Sv. This weaker offshore transport, measured on the western side of Belgica Trough, may indicate that a substantial fraction of the offshore transport occurs over the westernmost BellS continental shelf, west of Belgica Trough, which was not sampled during the cruise.

Integrating volume transport across the mid-shelf section (across both troughs) results in a net onshore transport of 0.66 ± 0.51 Sv (**Figure 10b**, middle panel). The lack of a closed volume budget may arise from not having the hydrographic transect extend to the coast in Latady Trough, and thus missing a topographically-steered circulation on the eastern side of this trough. By excluding station 45, at which the LADCP data recorded a strong southward flow, the imbalance is reduced to only 0.2 ± 0.5 Sv (**Figure 10b**, broken line). Alternatively, the 0.66 ± 0.51 Sv (onshore) imbalance could indicate that there are circulation pathways that carry water further to the west beyond our sampling region, for instance towards the Abbot Ice Shelf in an extension of the Antarctic Coastal Current.

The spatial distribution of heat transport follows a similar pattern to the volume transports. The magnitude of the heat transport is largest at the eastern side of Belgica Trough (**Figure 10a**). At the shelf break, 437 GW ± 86 GW enter the trough (stations 17 – 20; negative values imply southward heat transport). Due to large cancellations, the heat transport at the shelf break is balanced within the error, resulting in a net offshore transport of 43.2 ± 82.5 GW. At the mid-shelf section across Belgica and Latady troughs (**Figure 10c**), the heat transport has a net value of -370 GW ± 280 GW in Belgica Trough (southward transport) and a net 202 ± 97 GW in Latady Trough (northward transport). The cumulative heat transport across the entire mid-shelf section of Latady and Belgica troughs is -169 GW ± 118 GW, or a net heat transport towards the ice shelves. The calculation of errors here are somewhat uncertain (see discussion in **section 2.2**), and it is important to note that the net heat transport is small compared to onshore and offshore transports in each trough.

The thickness, h_{MCDW}, and heat content of the MCDW layer, $\mathcal{H}_{MCDW}$ (equation 3), at each station provide additional information about the locations where heat is transported onto the shelf and lost through a combination of interactions with ice shelf meltwater or via surface cooling. To estimate the thickness of the MCDW layer we use a temperature threshold of 1.1°C (**Figure 11**). The thickness and heat content of the MCDW layer is largest at the mouth of Belgica Trough and at the eastern side of Latady Trough. In Latady Trough, the MCDW thickness is uniform (h_{MCDW} ≈250 m), but its heat content presents a zonal gradient, with a larger heat content on the eastern side of the trough

(1.2 GJ m^{-2} versus 0.7 GJ m^{-2} at the western side, **Figure 11**). This suggests there is a significant meltwater contribution from the BellS ice shelves in Latady Trough that supports cooling and freshening of MCDW along its path towards the shelf break. The change in the heat content indicates that even within our MCDW class, defined by a temperature threshold, there are waters with various degrees of modification due to different amounts of meltwater.

In front of Venable Ice Shelf, stations 34 – 36 and 41 show a thick ($h_{MCDW} > 150$ m) yet cold MCDW layer. The western side of Belgica Trough hosts the thinnest MCDW layer ($h_{MCDW} \approx 50 - 75$ m) with the lowest heat content ($\mathcal{H}_{MCDW} = 0{-}0.2$ GJ m^{-2}). This further confirms the western side of Belgica Trough as the major pathway for meltwater mixtures exiting the BellS across the shelf break.

4 Discussion

4.1 Comparison to numerical models

The observations described above have allowed us to make the first quantitative estimates of the BellS continental shelf circulation. Therefore, the best points of comparison are with numerical models that have simulated the regional circulation of the West Antarctic coastal seas. A prominent feature of our observations is the transport of warm water towards the BellS ice shelves as well as the flow of waters, modified by glacial melt, away from the shelves via narrow boundary currents that are steered by bathymetry and have a lateral scale comparable to the station spacing $O(10{-}20$ km). This puts a strong constraint on the horizontal resolution needed to accurately capture physical processes that are controlling the continental shelf circulation (St-Laurent et al., 2013; Stewart & Thompson, 2015). It is not surprising then that early studies (*e.g.* Assmann et al. (2005); Holland et al. (2010)) only resolve a broad-scale cyclonic circulation that spans the entire continental shelf in the BellS. In particular, in Holland et al. (2010), the near-surface, two-dimensional streamfunction shows a circulation extending from the WAP, well north of Marguerite Trough, to the eastern boundary of the Amundsen Sea. At 200 m depth, their streamfunction shows more confinement to the BellS. Holland et al. (2010) do not provide an estimate of the depth-integrated transport over the continental shelf, although the annual mean horizontal streamfunction at 200 m peaks at roughly $5{\times}10^3$ m^2 s^{-1}. Assuming this value is uniform over an average depth of 500 m produces a volume transport of 2.5 Sv. This value is somewhat larger, but of comparable magnitude, to the total onshore transport calculated in Belgica and Latady troughs of roughly 1.5 Sv (**Figure 10**).

More recent modeling efforts have produced higher-resolution realizations of the BellS circulation and support the spatial variability in water properties apparent in our observations. In particular, Nakayama et al. (2014), analyzing output from a simulation with non-uniform grid spacing but less than 5 km resolution over the continental shelf, presents distinct fates for glacial MW entering from ice shelves located in the western and eastern parts of the BellS. Following a decade of integration, the largest MW content in the BellS is confined to Belgica Trough. This suggests (i) the importance of melt from ice shelves found along the southern edge of Eltanin Bay that are directly connected to Belgica Trough and (ii) the transfer of MW from Latady Trough into Belgica Trough before leaving the continental shelf. In this simulation, the MW is distributed broadly in Belgica Trough, rather than being confined to the western edge. Indeed, the regions of largest MW content are found on the eastern side of Eltanin Bay, suggesting the transport of MW from eastern ice shelves, such as George VI and Stange, towards the west. While the exact location of inter-trough exchange (between Belgica and Latady troughs) is difficult to discern from our observations, we did measure regions of enhanced flow where the bathymetric ridge separating the troughs is not as tall, for instance near stations 22 – 25 and 34 – 37 (**Figure 6c**). Our glacial MW estimates peak at the western boundaries of Belgica and Latady troughs, but we also find elevated meltwater fractions are spread broadly along density surfaces. Thus, both models and observations point to a significant degree of re-circulation over the continental shelf that may trap modified waters for up to decades, and would integrate changes in forcing, such as wind forcing at the shelf break, that impact shelf properties on shorter timescales (Walker et al., 2007; Jenkins et al., 2018).

The long-term fate of the glacial MW in Nakayama et al. (2014) is noteworthy. Despite its broad distribution within Belgica and Latady troughs, upon reaching the shelf break, the glacial MW predominantly flows westward. MW content is low over the continental slope of the WAP, suggesting little transfer to the east. Again, this is consistent with our observations that show large differences in MW fraction on the cross-slope sections at the western and eastern edges of the BellS. Additionally, the westward pathways appear to largely occur over the continental slope, in part due to the extremely shallow bathymetry to the north of Abbot Ice Shelf. To our knowledge, there are no ship-based observations in this region of the shelf due to persistent northerly winds producing packed sea ice conditions nearly year round. However, MW concentrations calculated using seal-based hydrographic data, were also low in this area (Zhang et al., 2016). Furthermore, numerical simulations in which MW was tracked from Abbot Ice Shelf showed limited export to other regions in West Antarctica, confirming the relative impermeability of the shallow shelf region to lateral exchange (Nakayama et al., 2014). It remains an open question as to whether a narrow coastal current connects the southern BellS to the eastern Amundsen Sea, perhaps even flowing under the Abbot Ice Shelf. Models will also be highly uncertain in this region due to a lack of high-resolution bathymetric data.

4.2 Comparison to the Amundsen Sea

In the Amundsen Sea, similar to the BellS, basal melt is driven by MCDW that enters the shelf via troughs (Webber et al., 2019; Dotto et al., 2019). While some studies have argued that the inflow of warm water, especially to the eastern-most trough, is a baroclinic process (Arneborg et al., 2012; Whlin et al., 2013), direct velocity observations have largely shown the vertical structure to be barotropic (Kalen et al., 2015; Biddle et al., 2019), similar to our observations in Belgica Trough. The horizontal volume transport within the eastern Amundsen Sea trough that feeds Pine Island Glacier was found to be 1.5 Sv (Thurnherr et al., 2014), roughly the same volume transport that flows towards the glaciers at the mid-shelf section spanning both BellS troughs. When considering the cumulative heat transport across Belgica Trough, our calculation of a net 0.5 TW at the mid-shelf station is much smaller than the 3.3 TW calculated in the Amundsen Sea (Webber et al., 2019), although note that these values will be sensitive to the ability to measure heat transport in narrow boundary currents near the coast. The net heat delivered by the shelf circulation should be considered in situations where the volume budget is closed, since the net heat flux is the residual of large terms flowing towards and away from the coast. Finally, MW is present across the entire continental shelf of the Amundsen Sea, with strong outflow at the western sides of two troughs (Biddle et al., 2019). This is consistent with our findings of MW across the entire BellS shelf and export pathways along the western sides of Belgica and Latady troughs. Considering the relatively small numbers of observations, it is difficult to comprehensively compare the MW distributions in the Amundsen Sea and the BellS. More locally, meltwater content, integrated vertically in the water column in front of Thwaites glacier, accumulates to as much as 4.5 m (Biddle et al., 2019), while this value peaks at 3.5 m in front of Venable Ice Shelf.

4.3 Variability of the regional circulation

This study provides one of the first hydrographic overviews of the entire BellS and suggests that this region plays a key role in integrating water modification processes throughout the West Antarctic coastal seas. The magnitude and spatial structure of the circulation in this study is largely consistent with the results of preliminary work done with inverse analysis approach applied to hydrographic data from 2007. Nevertheless, cautious interpretation of this data set is required due to our limited ability to assess temporal variability. On seasonal timescales, the numerical simulations of Mathiot et al. (2011) show that the frontal circulation over the continental shelf is susceptible to seasonal variability in the BellS, a result confirmed through satellite observations by Armitage et al. (2018). Changes in the wind stress and wind stress curl will almost certainly modify both the properties of MCDW and, perhaps more importantly, its thickness over the continental shelf, similar to variations observed in the Amundsen Sea (Dutrieux et al., 2014; Jenkins et al., 2018). Model studies have shown the importance of wind stress on the strength of the shelf-break jet, and hence the on-shelf heat transport of MCDW, since the jet greatly regulates such flow (Graham et al., 2016). Thus, comparing years when ship-based hydrographic data over the continental shelf are available (1994, 2007, 2019) – a focus of future work – will be challenging because data were collected at different times of the year. Data collected by instrumented seals is a promising resource for analyzing interannual variability, although this is hampered by the spatial heterogeneity in how the seals forage from year-to-year; they do not often return to the same spot. Still, combining these disparate data sets along with new remote sensing products (Armitage et al., 2018) should help to determine whether the BellS experiences similar shifts between warm and cold regimes that have been observed in the Amundsen Sea (Dutrieux et al., 2014; Jenkins et al., 2018).

Over longer timescales, however, there are features of the BellS that are distinct from the Amundsen Sea and relevant for the evolution of the circulation of the West Antarctic coastal seas. The Belgica, and likely, also the Latady troughs host an inflow of MCDW focused in deep troughs, similar to the Amundsen Sea, yet the eastern BellS additionally supports the inflow of a much lighter and fresher water mass related to the southward flow of the Antarctic Peninsula Coastal Current (Moffat & Meredith, 2018). This could influence the vertical stratification within the BellS as well as air-sea exchange, and in particular heat loss, in the large polynyas of the BellS in ways that are distinct from in the Amundsen Sea. Furthermore, due to the shallow bathymetry to the west of Belgica Trough, the outflow of modified waters is much more confined to the shelf break in the BellS (Thompson et al., 2020) than in the Amundsen Sea (Nakayama et al., 2017). This, in turn, could play an important role in setting properties of the Antarctic Slope Current. This is of interest as as the outflow from the BellS occurs at the confluence of the ACC's southern boundary and the eastern extent of the Ross Gyre, opening the possibility of the BellS circulation both responding to more remote forcing, such as the strength of the Ross Gyre. Finally, the Amundsen Sea and BellS may also in turn influence the structure of the Ross Gyre since the export of MW from the continental shelves contributes to establishing the frontal structure over the continental slope that forms the southern boundary of the gyre (Nakayama et al., 2018).

5 Summary

Observations collected in the Bellingshausen Sea (BellS) in austral summer 2018-19 are used to investigate the circulation over the continental shelf and this region's role in linking flow features throughout the West Antarctic coastal seas. Flow through the BellS connects the West Antarctic Peninsula seas (**Figure 1**), where MCDW on the continental shelf is warmest, to the Amundsen Sea where changes in the temperature of MCDW has been most pronounced (Schmidtko et al., 2014). Therefore, the circulation towards and away from floating ice shelves in the BellS will be a critical part of the larger region's response to a warming Southern Ocean. Relatively little is known about mechanistic controls on the BellS circulation features, in large part because dedicated observations in this region have been rare. A combination of ship-based and glider-based hydrography, along with lowered ADCP data, has provided a shelf-wide snapshot of this circulation as well as transports of heat and meltwater.

On the BellS shelf, MCDW is found mostly below 300 m. The warmest MCDW is found on the eastern side of Latady Trough, and this water mass cools progressively from east to west. There are multiple lines of evidence, including direct velocity measurements, meltwater concentrations, and heat transport estimates, showing that the observed cooling is indicative of modification through interaction with one or perhaps multiple ice shelves along the coast of the BellS. The signature of these modifications is most pronounced in water flowing offshore on the western edges of the two prominent troughs. This suggests that the ice shelf interactions support cyclonic lateral circulations in both Belgica and Latady troughs as well as an overturning in density space. The overturning circulation is evident through the change in density classes that host the denser, less-modified, onshore-flowing MCDW and the lighter, more-modified (*e.g.* higher meltwater concentrations), offshore-flowing MCDW. While meltwater is broadly distributed over the shelf, peak values are found immediately in front of Venable Ice Shelf and can be tracked, along density surfaces, towards the continental shelf break along the western edge of Belgica Trough.

The volume transport is nearly closed across both shelf-break and mid-shelf sections, suggesting that potential aliasing problems related to the "snapshot" nature of the LADCP observations (tidal velocities) are minimal. The cumulative transport, comparable to a horizontal streamfunction, reaches a maximum value of between 1 and 1.5 Sv in each trough, comparable to the circulation strength in the eastern Amundsen Sea. Due to the largely barotropic nature of the flow, we infer the baroclinic circulation, more closely linked to the overturning to be smaller (Whlin et al., 2020). The largest onshore heat transport occurs at the eastern side of both troughs. The thickness of the MCDW layer and its heat content also peak on the eastern side of each trough; the MCDW layer is progressively eroded and cooled while circulating inside the troughs (**Figure 11**).

While these observations improve our understanding of the BellS circulation, open questions remain. In particular, due to sea ice conditions during the cruise, we were not able to close the eastern boundary of Latady Trough, and the origin of the water flowing into this trough remains unclear. Future observations are needed to assess the link between inflow to the BellS and the Antarctic Coastal Current and how this can influence ice-shelf melt rates (Moffat et al., 2008; Kim, 2016). The processes that connect the circulations of the WAP (east of the BellS), the BellS continental shelf, and the Amundsen Sea (west of the BellS), and the time scales over which forcing anomalies are communicated between these regions, is an important avenue for further study. Such a connection would be a crucial piece in understanding heat and meltwater transport throughout the region. Based on the large-scale cyclonic circulation over the West Antarctic shelf (Assmann et al., 2005; Holland et al., 2010), this connection would imply that the circulation over the BellS continental shelf is influenced by physical processes along the Antarctic Peninsula that have been experiencing significant changes in response to a warming climate (Turner et al., 2005), while the circulation in the rapidly-evolving Amundsen Sea may be influenced by upstream processes in the BellS. The latter relationship is possible considering evidence in these observations that meltwater exported from the BellS shelf is directed into a slope current that, in turn, is directed towards the Amundsen Sea.

Acknowledgments
We acknowledge essential contributions from the captain and crew of the R/V Nathaniel B. Palmer as well as the Antarctic Support Contract staff during NBP19-01. This work was supported by the National Science Foundation. AFT, XR, and MF were supported by NSF OPP-1644172 and the David and Lucille Packard Foundation. LSC, KS, NS, RS, and CL were supported by NSF OPP-1643679. RO is supported by the COMPASS project from the European Research Council under the European Union's Horizon 2020 research

and innovation program (grant agreement n° 741120). We are grateful for comments from three reviewers that substantially improved this manuscript. All data used in this study are available at `https://data.nodc.noaa.gov/cgi-bin/iso?id=gov.noaa.nodc:0210639`.

Table 1. End member tracer values used for the optimal multiparameter analysis and meltwater fraction calculations. End members include Modified Circumpolar Deep Water (MCDW), Winter Water (WW) and meltwater (MW). Uncertainties ϵ and variance of the end-member tracer values were estimated from the spread in the end member values on property plots and are used to calculate the weights W_j following the discussion in section 2.3. W_4 is chosen to be 250 to ensure that any deviation away from 1 of the summed water mass fractions is at least an order of magnitude smaller than the meltwater fraction value.

	θ (°C)	S (psu)	O_2 (μmol kg^{-1})
End-member values			
MCDW	1.12	34.69	170
WW	-1.84	34.16	275
MW	-90.8	0	1125
Uncertainty parameters			
ϵ	1.2	0.1	400
σ	52.2	19.9	513
W	2274	3950	659

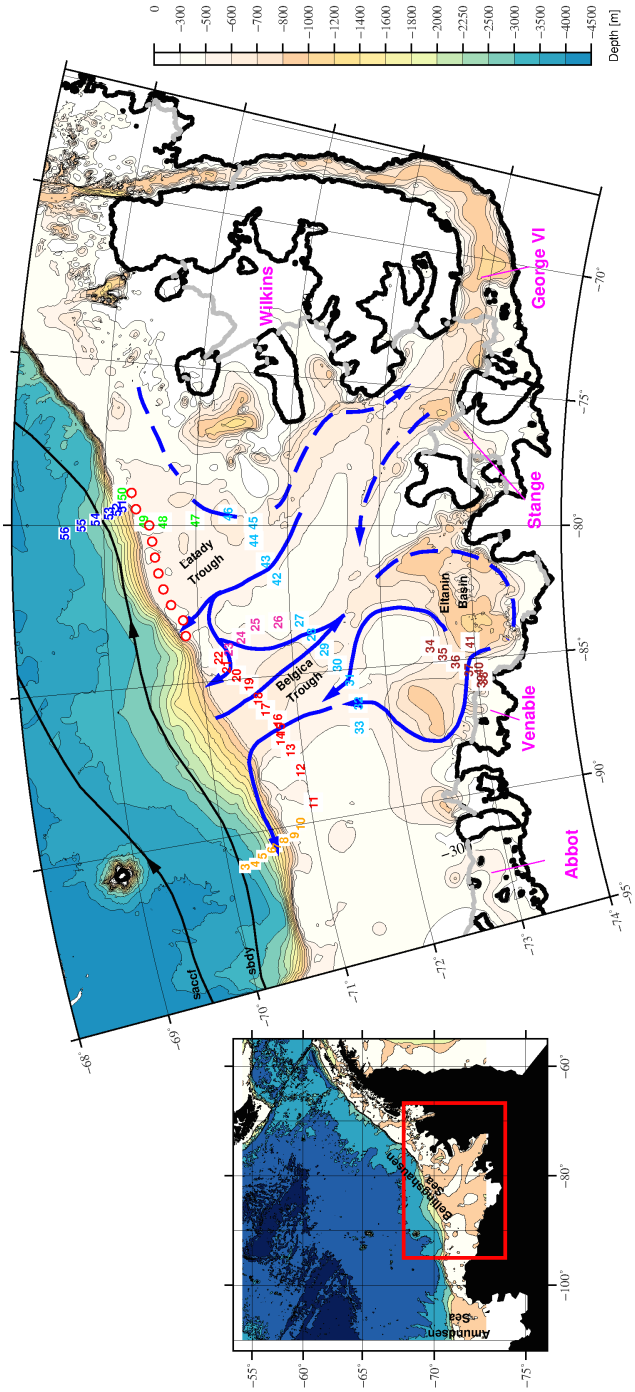

Figure 1. Map of the study region. (left) Overview of the West Antarctic coastal seas with the Bellingshausen Sea (BellS), located between the Amundsen Sea and the northern part of the West Antarctic Peninsula, indicated by the red box. (right) Bathymetry, hydrographic stations, and a schematic of the circulation in the BellS, inferred from this study. Ship-based Conductivity-Temperature-Depth (CTD) hydrographic stations (numbers) are indicated in colors that are used in subsequent figures. The glider hydrographic section is shown with red circles. A schematic of the circulation is given by the blue arrows, where solid and dashed lines show, respectively, currents directly resolved by velocity observations and currents inferred from water property distributions over the shelf. Positions of the southernmost fronts of the Antarctic Circumpolar Current (Orsi et al., 1995) (saccf = Southern Antarctic Circumpolar Current Front, sbdy = Southern Boundary) are shown as thin black lines (flow direction indicated with arrows). Bathymetry (m) is given in color from the RTopo-2 data product (Schaffer et al., 2016), and the coastline is indicated with a thick black line. Ice shelf fronts are shown with a thick gray line and the names of the ice shelves are given in pink. Bathymetry under the ice shelves is shown. The names of geographic features mentioned in the study are given in black (Belgica and Latady troughs, and the Eltanin Basin).

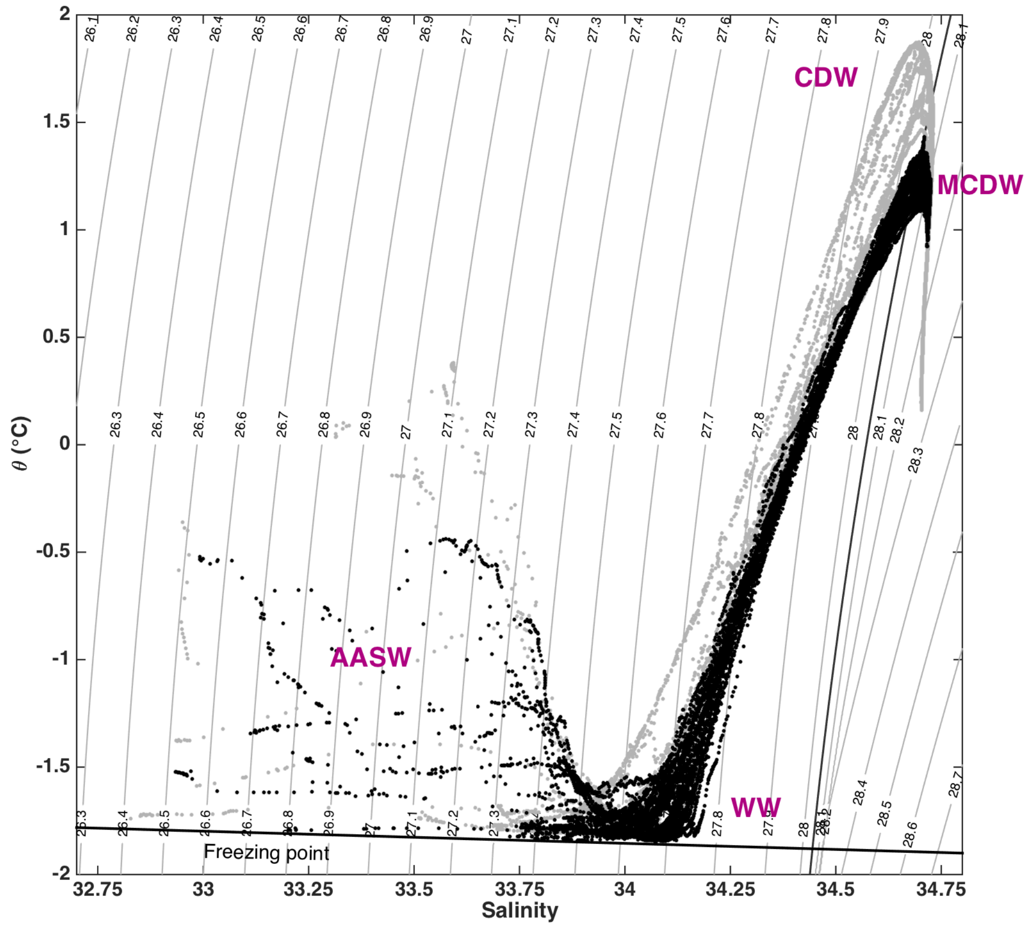

Figure 2. Potential Temperature-Salinity (θ-S) properties for all stations sampled on the BellS shelf (black), and CTD data across the slope (gray). The warmest offshore waters represent Circumpolar Deep Water (CDW), while all stations over the continental shelf at comparable densities have colder, modified properties we refer to as a MCDW. Both, on-shelf and offshore stations capture Winter Water (WW) and Antarctic Surface Water (AASW).

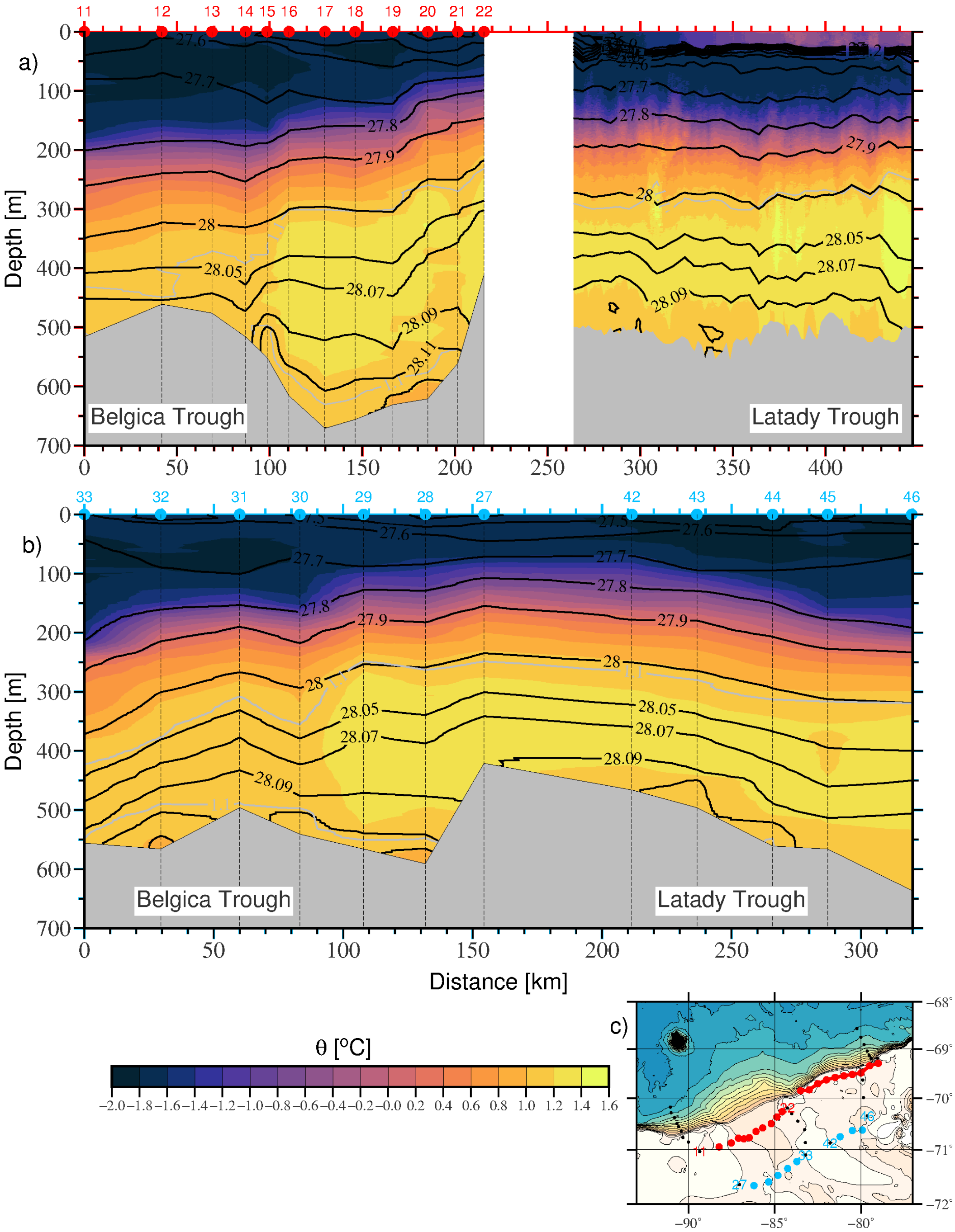

Figure 3. Potential temperature (color [°C]) sections with neutral density contours (black lines) spanning Belgica and Latady troughs. The data are plotted as distances from the westernmost station versus depth. (a) Potential temperature section at the shelf break in Belgica Trough (CTD stations 11 – 22, left) and Latady Trough from (glider data, right). Black vertical lines indicate the location of the stations. The 1.1°C isotherm, which bounds the MCDW layer, is shown as thin gray contours. Positions of glider dives are not shown since the data were smoothed and gridded before displaying. The raw glider data had a station spacing of roughly 4 km with 106 dives used in this panel. (b) Mid-shelf temperature section for Belgica (stations 33 – 27) and Latady (stations 42 – 46) troughs. (c) Map of the station positions with red and blue dots corresponding to panels (a) and (b), respectively. Station numbers are given in Figure 1.

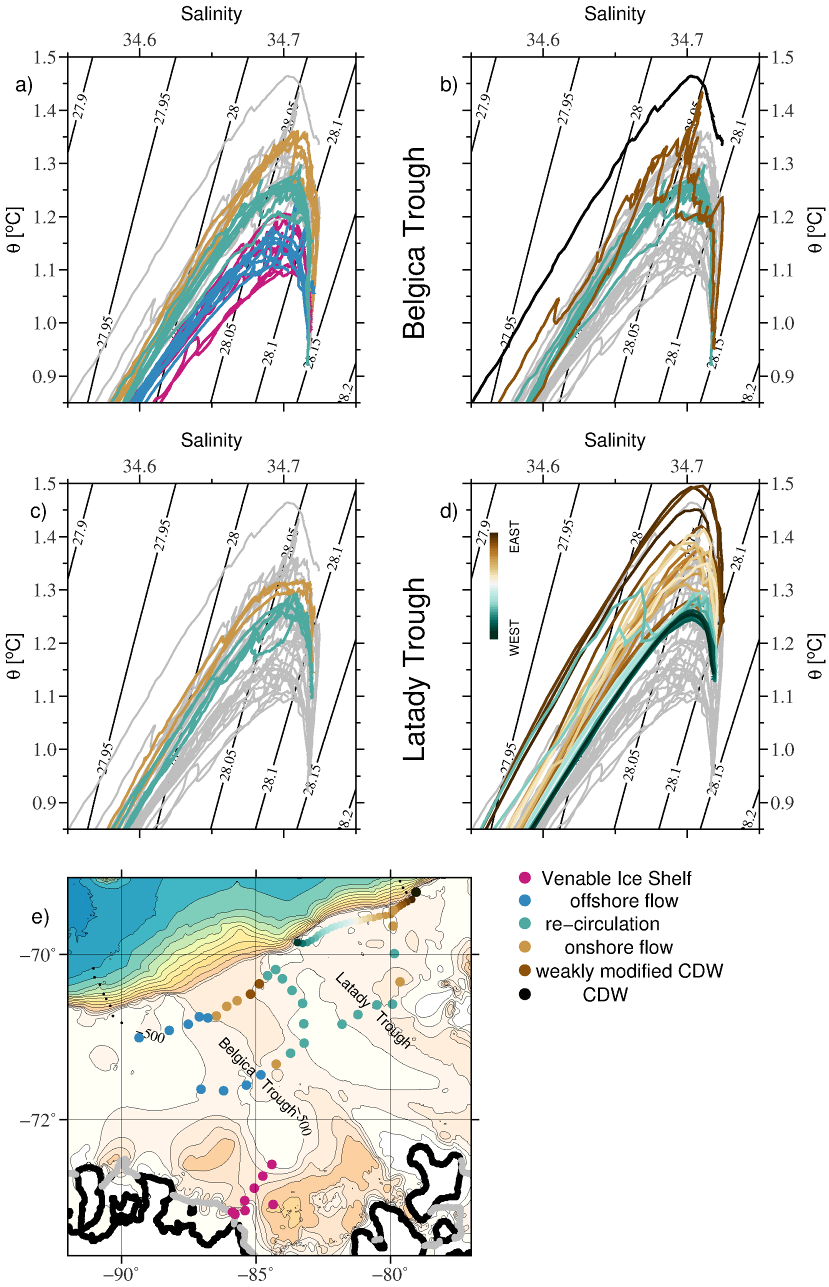

Figure 4. Potential temperature-salinity properties of Modified Circumpolar Deep Water (MCDW) in (a, b) Belgica Trough, as well as the eastern-most station in Latady Trough, and (c, d) Latady Trough. In each panel, all shelf stations (11 – 50) are shown in gray. In panels (a) and (b), stations in Belgica Trough (St. 11 – 22, 27 – 33), stations that connect the two troughs (St. 23 – 26), stations in front of Venable Ice Shelf (St. 34 – 41), and the eastern-most station in Latady Trough (St. 50) are color coded by degree of MCDW modification. Stations colored violet indicate glacially-modified MCDW, blue indicates MCDW flowing offshore, green indicated MCDW related to re-circulation on the shelf, light brown indicates MCDW flowing onshore near the shelf break, and dark brown indicates MCDW with offshore characteristics (e.g. little or no modification); panels (a, b) highlight stations with a greater and less degree of modification in the MCDW water mass, respectively. (c) As in panels (a, b) but for MCDW in Latady Trough (stations 42 – 49). (d) As in panels (a, b) but for profiles obtained from the glider; there is a clear signature of MCDW becoming progressively more modified as the glider sampled from west to east along this transect as shown by the legend. (e) All stations are shown on the map in the color that represents their MCDW properties.

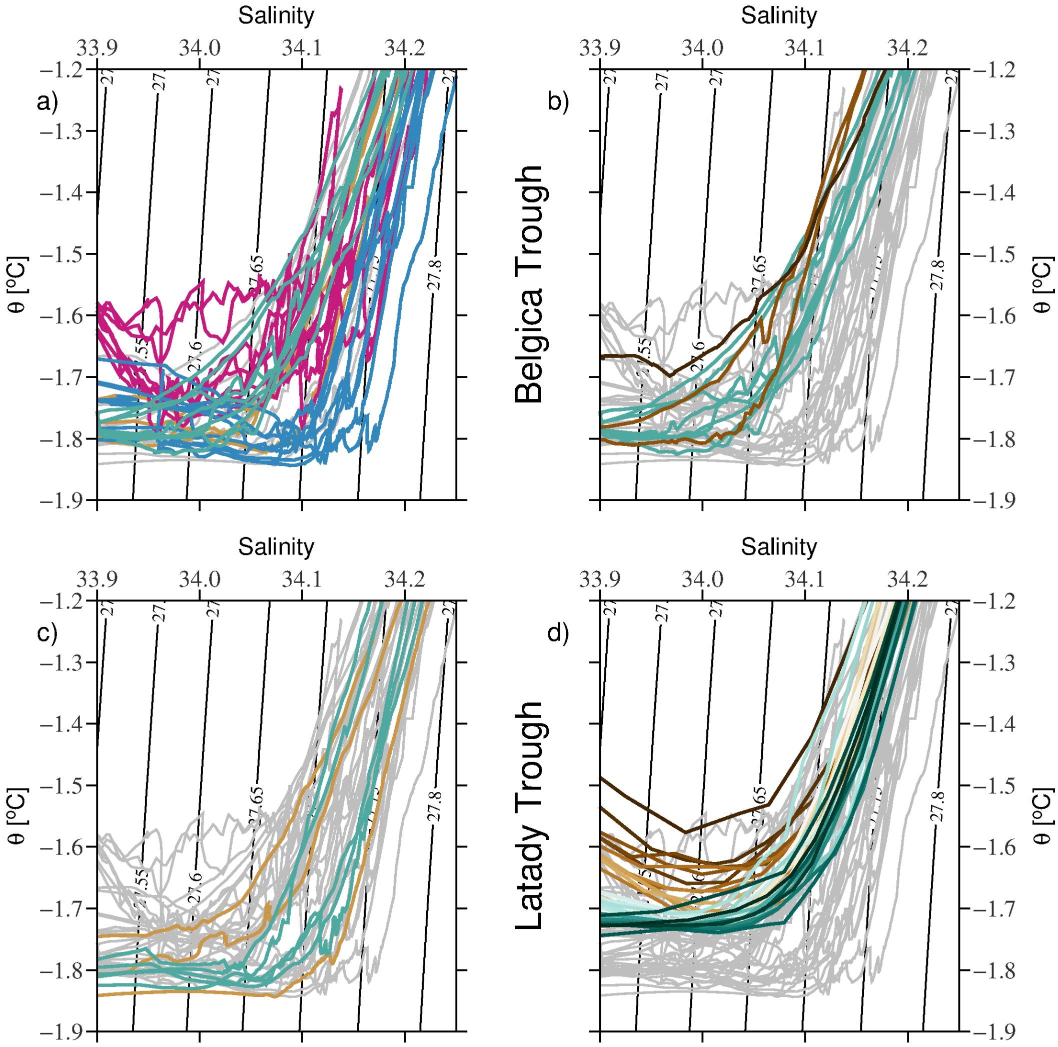

Figure 5. As in Figure 4, but for potential temperature-salinity properties of Winter Water (WW).

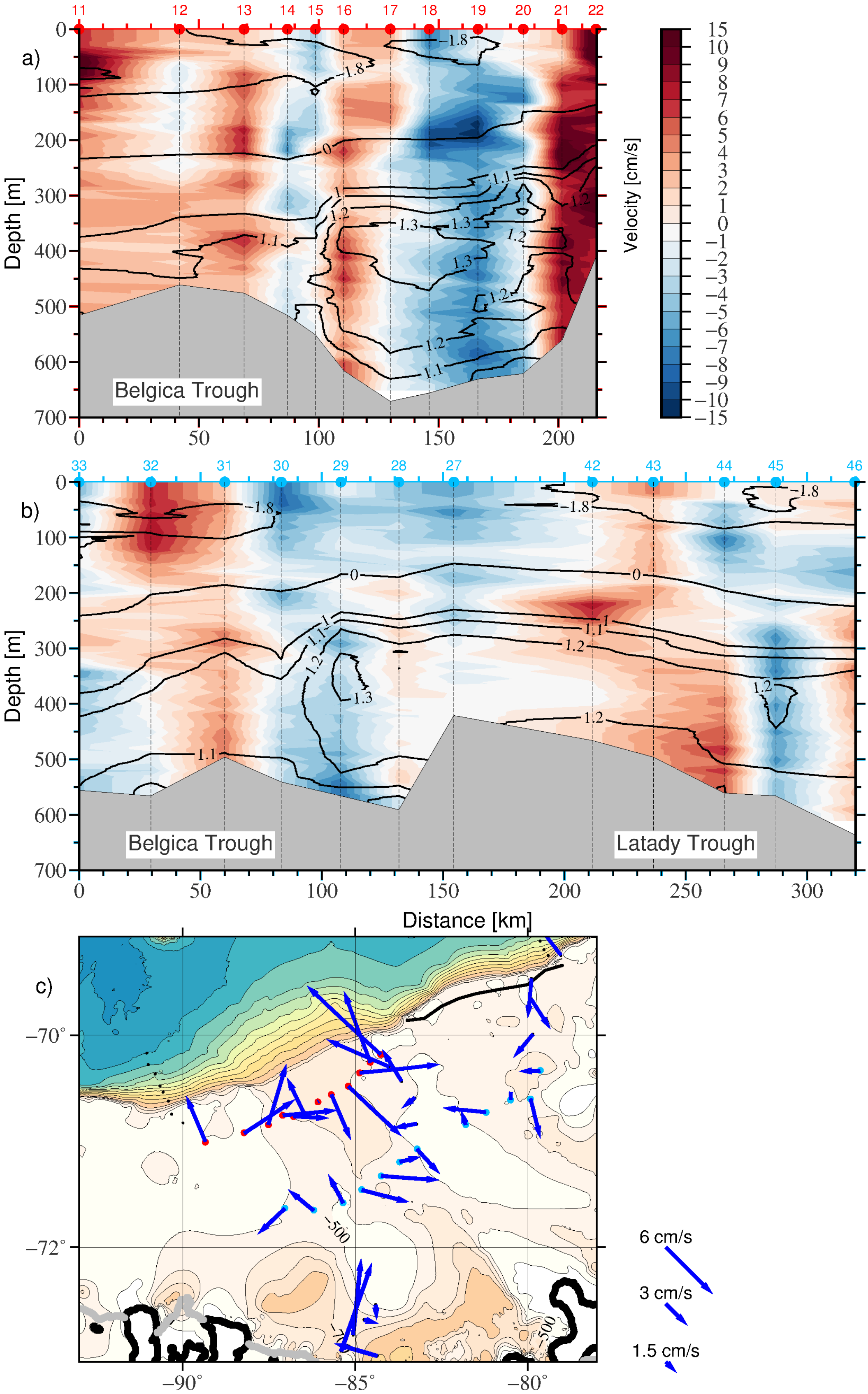

Figure 6. LADCP velocity data for (a) Belgica Trough (shelfbreak) section and (b) Belgica and Latady troughs (mid-shelf) section. Velocity estimates from the glider are not available. Velocities (cm s^{-1}) shown in each transect are rotated to be perpendicular to the section. Positive velocities (red) are directed offshore, negative velocities (blue) are directed on to the shelf. Temperature contours are shown in black. Panel (c) shows the depth-averaged velocities at each station from the LADCP data (blue arrows).

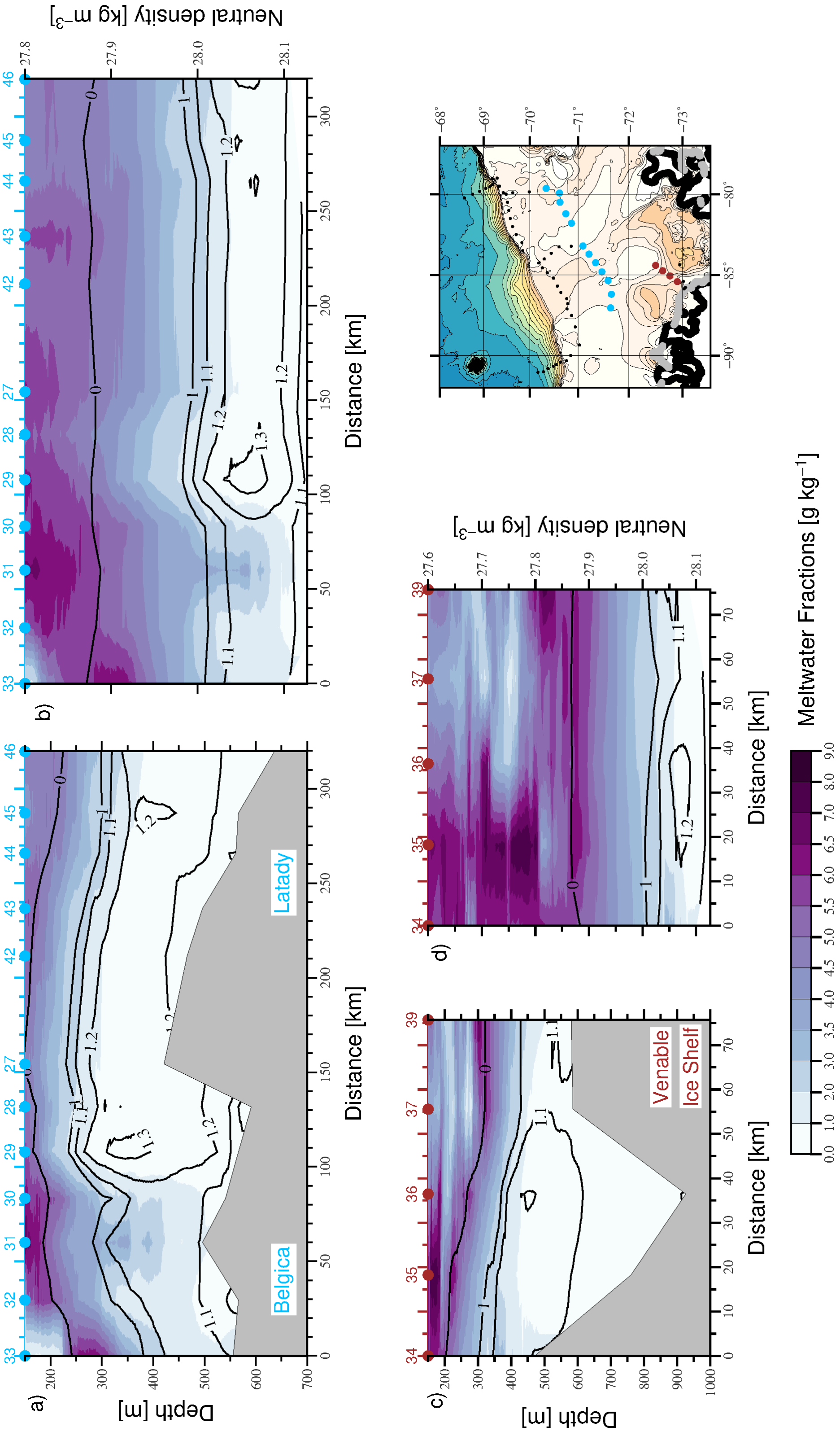

Figure 7. Meltwater fractions (g kg^{-1}, color) in Belgica and Latady troughs overlaid with temperature contours. The sections are shown in distance vs. depth starting below 150 m (a and c) and distance vs. density (b and d). The upper 150 m are excluded from the figures to eliminate signals due to surface forcing. The sections show distributions across the (a-b) Belgica and Latady troughs (mid-shelf section) and (c-d) in front of Venable Ice Shelf. For the latter transect, Venable Ice Shelf is located ∼2 km away from station 39 (right side of panels c, d). All stations are color coded and shown on the map.

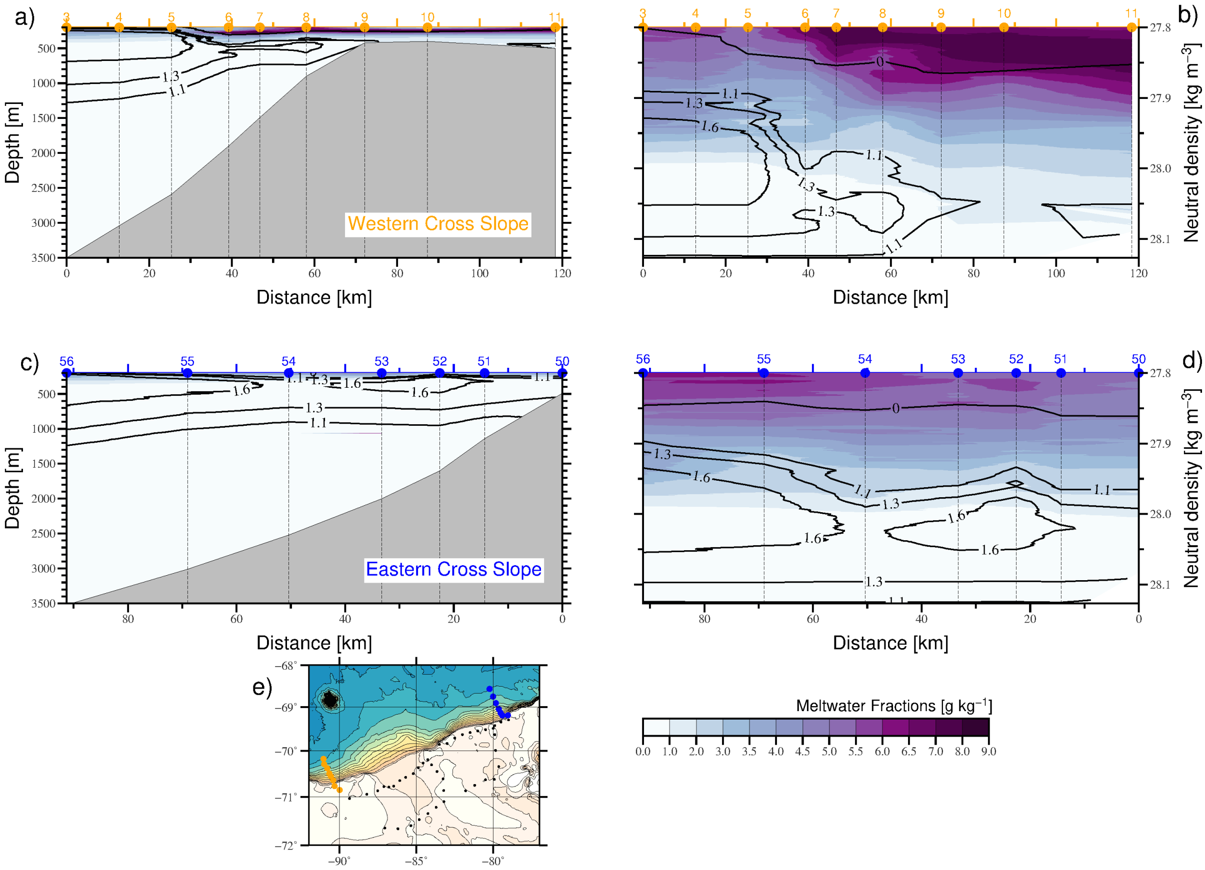

Figure 8. Meltwater fractions (g kg^{-1}, color) along the sections spanning the continental slope west of Belgica Trough (a, b) and east of Latady Trough (c, d). The sections are shown in distance vs. depth starting below 150 m (a, c) and distance vs. density (b, d). The location of the sections is shown in the map in panel (e).

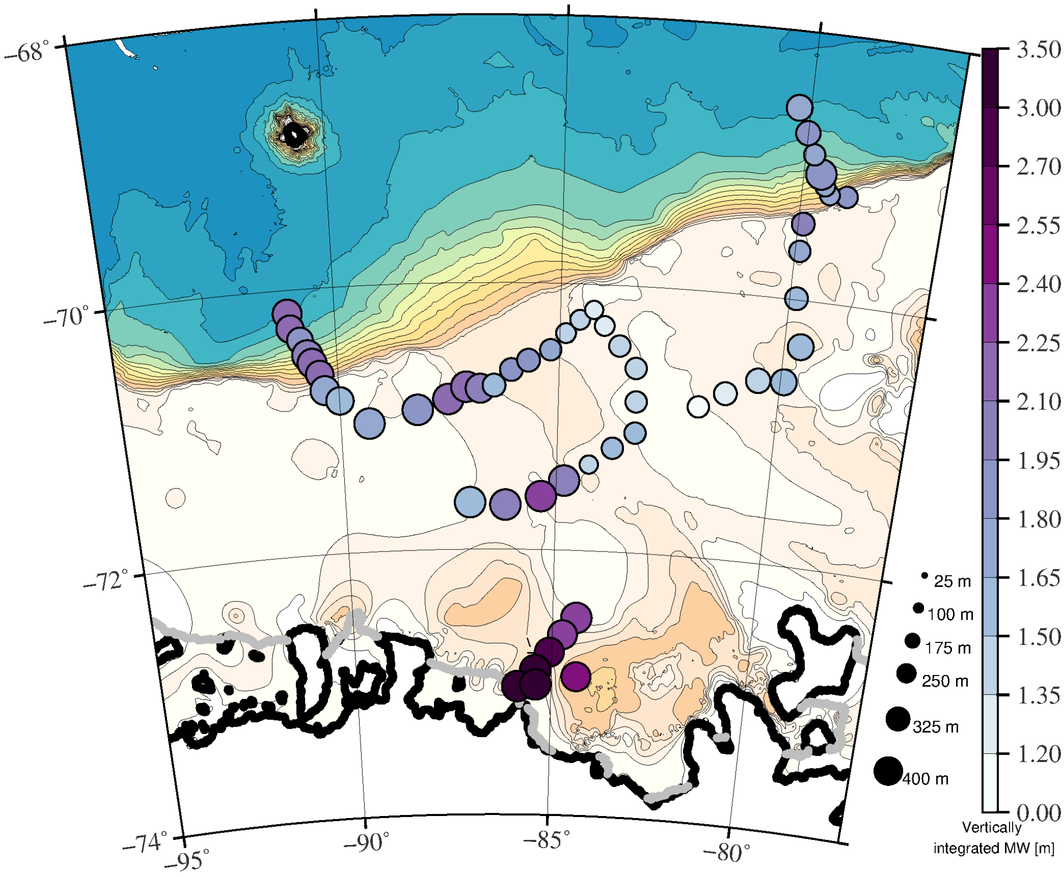

Figure 9. Map of meltwater distribution in the BellS based on the thickness (m, size of circles) and vertically-integrated meltwater content (m, color) for each station, below 150 m. The thickness is calculated as the part of the water column having a meltwater fraction greater than 1 g kg^{-1}. The bathymetry (m) is given in color as in Figure 1. Note the non-linear colorbar.

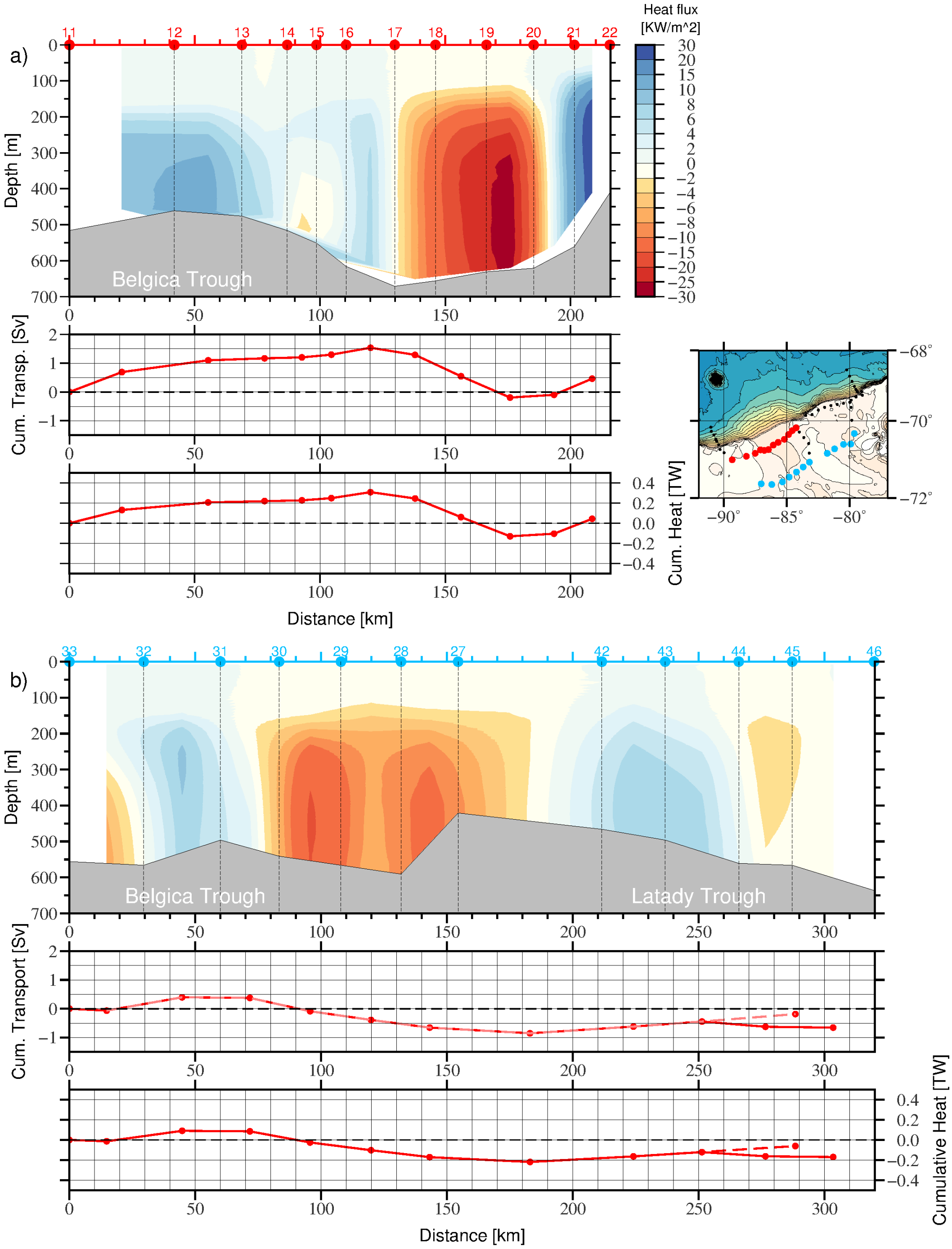

Figure 10. Volume and heat transport estimates for Belgica and Latady troughs based on LADCP-referenced geostrophic velocities. a) Distribution of heat flux (KW/m^2) across the mouth of Belgica Trough (color, stations 11 – 22), calculated as in equation (1). The panels below show the cumulative volume transport (Sv) and the cumulative heat transport (TW) across the same section. b) Same as in panel a), but for the mid-shelf section that spans Belgica (stations 27–33) and Latady (stations 42–26) troughs. The inset map shows the location of the sections in panels a) (red) and b) (blue).

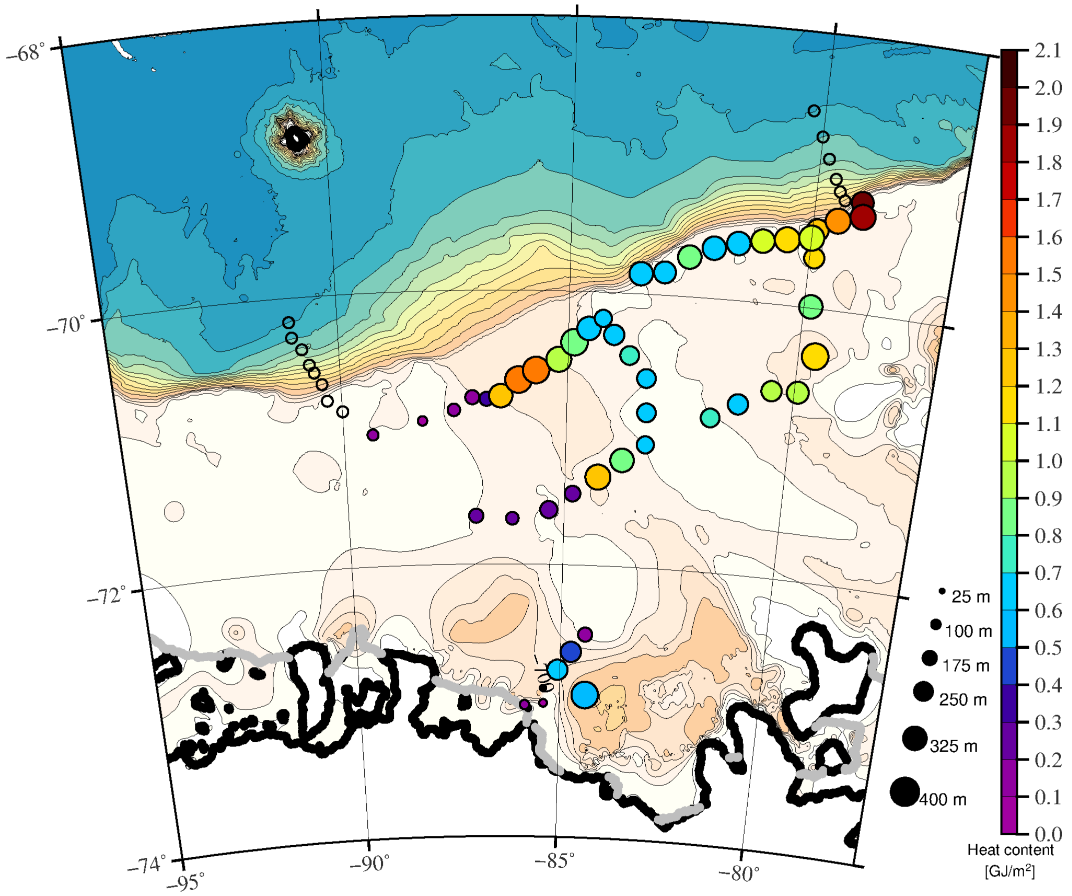

Figure 11. Map showing the thickness of the MCDW layer (m, size of circles) and its heat content (GJ m^{-2}, color) for each station. The MCDW layer is defined as the part of the water column where temperatures exceed 1.1°C. The heat content of this layer is calculated using equation (3).

References

Adusumilli, S., Fricker, H. A., Medley, B., Padman, L., & Siegried, M. R. (2020). Interannual variations in meltwater input to the Southern Ocean from Antarctic ice shelves. *Nat. Geosci.*, *13*, 616–620.

Armitage, T. W. K., Kwok, R., Thompson, A. F., & Cunningham, G. (2018). Dynamic topography and sea level anomalies of the Southern Ocean: Variability and teleconnections. *J. Geophys. Res.*, *123*, 613 – 630. doi: 10.1002/2017JC013534

Arneborg, L., Wåhlin, A. K., Björk, G., Liljebladh, B., & Orsi, A. (2012). Persistent inflow of warm water onto the central Amundsen shelf. *Nat. Geosci.*, *5*, 876–880. doi: 10.1038/ngeo1644

Assmann, K., Hellmer, H. H., & Jacobs, S. S. (2005). Amundsen Sea ice production and transport. *J. Geophys. Res*, *110*, C12013.

Beaird, N., Straneo, F., & Jenkins, W. J. (2015). Spreading of Greenland meltwaters in the ocean revealed by noble gases. *Geophys. Res. Lett.*, *42*, 7705 – 7713.

Biddle, L. C., Heywood, K. J., Kaiser, J., & Jenkins, A. (2017). Glacial meltwater identification in the Amundsen Sea. *J. of Phys. Oceanorg.*, *47*, 933–954.

Biddle, L. C., Loose, B., & Heywood, K. J. (2019). Upper ocean distribution of glacial meltwater in the Amundsen Sea, Antarctica. *J. Geophys. Res.*, *124*, 6854 – 6870. doi: 10.1029/2019JC015133

Brearley, J. A., Moffat, C., Venables, H. J., Meredith, M. P., & Dinniman, M. S. (2019). The role of eddies and topography in the export of shelf waters from the West Antarctic Peninsula shelf. *J. Geophys. Res. Oceans*, *124*. doi: 10.1029/2018JC0146795

Cook, A., Holland, P., Meredith, M., Murray, T., Luckman, A., & Vaughan, D. (2016). Ocean forcing of glacier retreat in the western Antarctic Peninsula. *Science*, *353*, 283–286.

Cook, A., & Vaughan, D. (2010). Overview of areal changes of the ice shelves on the Antarctic Peninsula over the past 50 years. *Cryosphere*, *4*, 77–98.

Couto, N., Martinson, D. G., Kohut, J., & Schofield, O. (2017). Distribution of Upper Circumpolar Deep Water on the warming continental shelf of the West Antarctic Peninsula. *J. Geophys. Res. Oceans*, *122*, 5306 – 5315. doi: 10.1002/2017JC012840

Dinniman, M., & Klinck, J. (2004). A model study of circulation and cross-shelf exchange on the west Antarctic Peninsula continental shelf. *Deep Sea Res. II*, *51*(17-19), 2003–2022.

Dinniman, M., Klinck, J., & Smith Jr., W. (2011). A model study of Circumpolar Deep Water on the West Antarctic Peninsula and Ross Sea continental shelves. *Deep Sea Res. II*, *58*, 1508–1523.

Dotto, T. S., Garabato, A. C. N., Bacon, S., Holland, P. R., Kimura, S., Firing, Y. L., ... Jenkins, A. (2019). Wind-driven processes controlling oceanic heat delivery to the Amundsen Sea, Antarctica. *J. Phys. Oceanogr.*, *49*, 2829 – 2849. doi: 10.1175/JPO-D-19-0064.1

Dutrieux, P., Rydt, J. D., Jenkins, A., Holland, P., Ha, H. K., Lee, S. H., ... Schroeder, M. (2014). Strong sensitivity of Pine Island ice-shelf melting to climatic variability. *Science*, *343*, 174 – 178. doi: 10.1126/science.1244341

Gade, H. G. (1979). Melting of ice in sea water: a primitive model with application to the Antarctic Ice Shelf and icebergs. *J. Phys. Oceanogr.*, *9*, 1890 – 198.

Garau, B., Ruiz, S., Zhang, W. G., Pascual, A., Heslop, E., Kerfoot, J., & Tintore, J. (2011). Thermal lag correction on Slocum CTD glider data. *J. Atmos. Oceanic Tech.*, *28*, 1065–1071. doi: https://doi:10.1175/JTECH-D-10-05030.1

Gille, S. T. (2008). Decadal-scale temperature trends in the Southern Hemisphere ocean. *J. Climate*, *21*(18), 4749–4765.

Graham, J. A., Dinniman, M. S., & Klinck, J. M. (2016). Impact of model resolution for on-shelf heat transport along the West Antarctic Peninsula. *J. Geo-*

phys. Res. Oceans, *121*, 7880 – 7897. doi: 10.1002/2016JC11875
Holland, P. R., Jenkins, A., & Holland, D. M. (2010). Ice and ocean processes in the Bellingshausen Sea, Antarctica. *J. Geophys. Res.*, *115*, C05020. doi: 10.1029/2008JC005219.
Howard, S. L., Padman, L., & Erofeeva, S. (2019). Cats2008: Circum-antarctic tidal simulation version 2008. *U.S. Antarctic Program (USAP) Data Center*. doi: https://doi.org/10.15784/601235
IMBIE. (2018). Mass balance of the Antarctic Ice Sheet from 1992 to 2017. *Nature*, *558*, 219–222.
Jacobs, S. S. (1991). On the nature and significance of the Antarctic Slope Front. *Mar. Chem.*, *35*, 9–24.
Jenkins, A., & Jacobs, S. S. (2008). Circulation and melting beneath George VI Ice Shelf, Antarctica. *J. Geophys. Res.*, *113*, C04013. doi: 10.1029/2007JC004449
Jenkins, A., Shoosmith, D., Dutrieux, P., Jacobs, S., Kim, T. W., Lee, S. H., ... Stammerjohn, S. (2018). West Antarctic Ice Sheet retreat in the Amundsen Sea driven by decadal oceanic variability. *Nature Geosci*, *11*, 733 - 738. doi: 10.1038/s41561-018-0207-4
Joughin, I., Tulaczyk, S., Bindschadler, R., & Price, S. (2002). Changes in West Antarctic ice stream velocities: observation and analysis. *J. Geophys. Res.*, *107*. doi: 10.1029/2001JB001029
Kalen, O., Assmann, K. M., Whlin, A. K., Ha, H., Kim, T. W., & Lee, S. (2015). Is the oceanic heat flux on the central Amundsen Sea shelf caused by barotropic or baroclinic currents? *Deep-Sea Res. II*, *123*, 7 – 15. doi: 10.1016/j.dsr2.2015.07.014
Kim, I. (2016). The distribution of glacial meltwater in the Amundsen Sea, Antarctica. *J. Geophys. Res.*, *121*, 1654–1666.
Loose, B., & Jenkins, W. J. (2014). The five stable noble gases are sensitive unambiguous tracers of glacial meltwater. *Geophys. Res. Lett.*, *41*, 2835 – 2841.
Loose, B., Schlosser, P., Smethie, W. M., & Jacobs, S. (2009). An optimized estimate of glacial melt from the Ross Ice Shelf using noble gases, stable isotopes and CFC transient tracers. *J. Geophys. Res.*, *114*, C08007. doi: 10.1029/2008JC005048
Mathiot, P., Goosse, H., Fichefet, T., Barnier, B., & Gallee, H. (2011). Modelling the seasonal variability of the Antarctic Slope Current. *Ocean Science, European Geoscience Union*, *7*, 445 – 532. doi: 10.5194/os-7-455-2011
McTaggart, K. E., Johnson, G. C., Johnson, M. C., Delahoyde, F., & Swift, J. H. (2010). Notes on CTD/O data acquisition and processing using Sea-Bird hardware and software. *IOCCP Reports*, *Report No. 14*, ICPO Publication Series No. 134. (Version 1)
Moffat, C., Beardsley, R. C., Owens, B., & Van Lipzig, N. (2008). A first description of the Antarctic Peninsula Coastal Current. *Deep Sea Res. Part II*, *55*, 277–293.
Moffat, C., & Meredith, M. (2018). Shelf-ocean exchange and hydrography west of the Antarctic Peninsula: a review. *Phil. Trans. Roy. Soc. A*, *376*, 20170164. doi: 10.1098/rsta.2017.0164
Moffat, C., Owens, B., & Beardsley, R. C. (2009). On the characteristics of Circumpolar Deep Water intrusions to the west Antarctic Peninsula Continental Shelf. *J. Geophys. Res.*, *114*, C05017. doi: 10.1029/2008JC004955
Morlighem, M., et al. (2019). MEaSUREs BedMachine Antarctica, Version 1. *Boulder, Colorado USA. NASA National Snow and Ice Data Center Distributed Active Archive Center*. doi: https://doi.org/10.5067/C2GFER6PTOS4
Mosby, H. (1934). The waters of the Atlantic Antarctic Ocean. *The Norwegian Antarctic Expeditions*, *1*, 131.
Nakayama, Y., Menemenlis, D., Schodlok, M., & Rignot, E. (2017). Amundsen and Bellingshausen Seas simulation with optimized ocean, sea ice, and thermody-

namic ice shelf model parameters. *J. Geophys. Res.*, *122*, 6180–6195.

Nakayama, Y., Menemenlis, D., Zhang, H., Schodlok, M., & Rignot, E. (2018). Origin of Circumpolar Deep Water intruding onto the Amundsen and Bellingshausen Sea continental shelves. *Nat. Comm.*, *9:3403*, 1 – 9.

Nakayama, Y., Schröder, M., & Hellmer, H. H. (2013). From circumpolar deep water to the glacial meltwater plume on the eastern Amundsen shelf. *Deep Sea Res. Part I*, *77*, 50–62.

Nakayama, Y., Timmermann, R., Rodehacke, C. B., Schröder, M., & Hellmer, H. H. (2014). Modeling the spreading of glacial meltwater from the Amundsen and Bellingshausen seas. *Geophys. Res. Lett.*, *41*(22), 7942–7949.

Naveira-Garabato, A. C., Forryan, A., Dutrieux, P., Brannigan, L., Biddle, L. C., Heywood, K. J., ... S., K. (2017). Vigorous lateral export of the meltwater outflow from beneath an Antarctic ice shelf. *Nature*, *542*, 219 – 222. doi: 10.1038/nature20825

Orsi, A. H., Whitworth III, T., & Nowlin Jr., W. D. (1995). On the meridional extent and fronts of the Antarctic Circumpolar Current. *Deep Sea Res. I*, *42*, 641–673.

Padman, L., Costa, D. P., Dinniman, M. S., Fricker, H. A., Goebel, M. E., Huckstadt, L. A., ... van den Broeke, M. R. (2012). Oceanic controls on the mass balance of Wilkins Ice Shelf, Antarctica. *J. Geophys. Res. Oceans*, *117*. doi: 10.1029/2011JC007301

Padman, L., Fricker, H. A., R. Coleman, S. H., & Erofeeva, L. (2002). A new tide model for the Antarctic ice shelves and seas. *Annals of Glaciology*, *34*, 247 – 254.

Paolo, F. S., Fricker, H. A., & Padman, L. (2015). Volume loss from Antarctic ice shelves is accelerating. *Science*, *348*, 327–331.

Pea-Molino, B., McCartney, M. S., & Rintoul, S. (2016). Direct observations of the Antarctic Slope Current transport at 113$^{\mathrm{oE}}$. *J. Geophys. Res.*, *121*, 7390 – 7407. doi: 10.1002/2015JC011594

Pritchard, H. D., Ligtenberg, S. R. M., Fricker, H. A., Vaughan, D. G., van den Broeke, M. R., & Padman, L. (2012, 04 26). Antarctic ice-sheet loss driven by basal melting of ice shelves. *Nature*, *484*(7395), 502–505. Retrieved from http://dx.doi.org/10.1038/nature10968

Richardson, G., Wadley, M. R., Heywood, K. J., Stevens, D. P., & Banks, H. T. (2005). Short-term climate response to a freshwater pulse in the Southern Ocean. *Geophys. Res. Lett.*, *32*, L03702. doi: 10.1029/2004GL021586

Rignot, E., Jacobs, S., Mouginot, J., & Scheuchl, B. (2013). Ice-shelf melting around Antarctica. *Science*, *341*, 266–270.

Rignot, E., Mouginot, J., Morlighem, M., Seroussi, H., & Scheichl, B. (2014). Widespread, rapid grounding line retreat of Pine Island, Thwaites, Smith, and Kohler glaciers, West Antarctica, from 1992 to 2011. *Geophys. Res. Lett*, *41*, 3502–3509.

Rignot, E., Mouginot, J., Scheuchl, B., van den Broeke, M., van Wessem, M. J., & Morlighem, M. (2019). Four decades of Antarctic Ice Sheet mass balance from 1979 – 2017. *PNAS*, *116*, 1095–1103.

Rye, C. D., Naveira-Garabato, A. C., Holland, P. R., Meredith, M. P., Nurser, A. J. G., Hughes, C. W., ... Webb, D. J. (2014). Rapid sea-level rise along the Antarctic margins in response to increased glacial discharge. *Nat. Geosci.*, *7*, 732–735. doi: 10.1038/ngeo2230

Savidge, D. K., & Amft, J. A. (2009). Circulation on the west Antarctic Peninsula derived from 6 years of shipboard adcp transects. *Deep Sea Res. I*, *56*, 1633–1655.

Schaffer, J., Timmermann, R., Arndt, J. E., Kristensen, S. S., Mayer, C., Morlighem, M., & Steinhage, D. (2016). A global, high-resolution data set of ice sheet topography, cavity geometry, and ocean bathymetry. *Earth Syst.*

Sci. Data, *8*, 542-557.
Schmidtko, S., Heywood, K., Thompson, A., & Aoki, S. (2014). Multidecadal warming of Antarctic waters. *Science*, *346*, 1227-1231.
Smith, B., Fricker, H. A., Gardner, A. S., Medley, B., Nilsson, J., Paolo, F. S., ... Zwally, H. J. (2020). Pervasive ice sheet mass loss reflects competing ocean and atmopshere processes. *Science*, *368*, 1239-1242.
Stewart, A., & Thompson, A. (2015). Deep Water across the Antarctic shelf break. *Geophys. Res. Lett.*, *42*, 432–440.
St-Laurent, P., Klinck, J. M., & Dinniman, M. S. (2013). On the role of coastal troughs in the circulation of warm circumpolar deep water on Antarctic Shelves. *J. Phys. Oceanogr.*, *43*, 51 – 64. doi: 10.1175/JPO-D-11-0237.1
Swart, N. C., & Fyfe, J. C. (2013). The influence of recent Antarctic ice sheet retreat on simulated sea ice area trends. *Geophys. Res. Lett.*, *40*, 4328–4332.
Talbot, M. H. (1988). Oceanic environment of George VI Ice Shelf, Antarctic Peninsula. *Ann. Glaciol.*, *11*, 161–164.
Thompson, A., Speer, K. G., & Schulze Chretien, L. M. (2020). Genesis of the Antarctic Slope Current in West Antarctica. *Geophys. Res. Let.*, *47*. doi: 10.1029/2020GL087802
Thompson, A., Stewart, A. L., Spence, P., & Heywood, K. J. (2018). The Antarctic Slope Current in a changing climate. *Reviews of Geophysics*, *56*, 741 – 770. doi: 10/10292018RG000624
Thurnherr, A. M., Jacobs, S. S., Dutrieux, P., & Giulivi, C. F. (2014). Export and circulation of ice cavity water in Pine Island Bay. *J. Geophys. Res. Oceans*, *119*, 1754 – 1764. doi: 10.1002/2013JC009307
Thurnherr, A. M., Visbeck, M., Firing, E., King, B. A., Hummon, J. M., Krahmann, G., & Huber, B. (2010). A manual for acquiring Lowered Doppler Current Profilier data. *In The GO-SHIP Repeat Hydrography Manual: A Collection of Expert Reports and Guidelines*, *Version 1, (eds E. M. Hood, C. L. Sabine and B. M. Sloyan*, 21. (IOCCP Report Number 14; ICPO Publication Series Number 134))
Tomczak, M. (1981). A multi-parameter extension of temperature/salinity diagram techniques for the analysis of non-isopycnal mixing. *Prog. Oceanogr.*, *10*, 147 – 171.
Turner, J., Colwell, S. R., Marshall, G. J., Lachlan-Cope, T. A., Carleton, A. M., Jones, P. D., ... Iagovkina, S. (2005). Antarctic climate change during the last 50 years. *Int. J. Climatol.*, *25*, 279-294.
Walker, D. P., Brandon, M., Jenkins, A., Allen, J. T., Dowdeswell, J., & Evans, J. (2007). Oceanic heat transport onto the Amundsen Sea shelf through a submarine glacial trough. *Geophys. Res. Let.*, *34*, L02602. doi: 10.1029/2006GL028154
Walker, D. P., Jenkins, A., Assmann, K. M., Shoosmith, D. R., & Brandon, M. A. (2013). Oceanographic observations at the shelf break of the Amundsen Sea, Antarctica. *J. Geophys. Res.*, *118*, 2906–2918.
Webber, B. G. M., Heywood, K. J., Stevens, D. P., & Assmann, K. M. (2019). The impact of overturning and horizontal circulation in Pine Island Trough on ice shelf melt in the eastern Amundsen Sea. *J. Phys. Oceanogr.*, *49*(1), 63 – 83. doi: 10.1175/JPO-D-17-0213.1
Whitworth III, T., Orsi, A. H., Kim, S.-J., Nowlin Jr., W. D., & Locarnini, R. A. (1998). Water masses and mixing near the Antarctic Slope Front. *In Ocean, Ice, and Atmosphere: Interactions at the Antarctic Continental Margin, (eds S.S. Jacobs and R.F. Weiss)*. doi: 10.1029/AR07p0001
Whlin, A. K., Kalen, O., Arneborg, L., Bjrk, G., Carvajal, G., Ha, H. K., ... Stranne, C. (2013). Variability of warm deep water inflow in a submarine trough on the Amundsen Sea Shelf. *J. Phys. Oceanogr.*, *43*(10), 2054 – 2070. doi: 10.1175/JPO-D-12-0157.1

Whlin, A. K., Steige, N., Darelius, E., Assmann, K. M., Glessmer, M. S., Ha, H. K., … Viboud, S. (2020). Ice front blocking of ocean heat transport to an Antarctic ice shelf. *Nature*, *578*, 568–571. doi: https://doi.org/10.1038/s41586-020-2014-5

Zhang, X., Thompson, A. F., Flexas, M. M., Roquet, F., & Bornemann, H. (2016). Circulation and meltwater distribution in the Bellingshausen Sea: from shelf break to coast. *Geophys. Res. Lett*, *43*, 6402 – 6409. doi: 10.1002/2016GL068998